The Role of Liquefaction on the Seismic Response of Quay Walls during the 2014 Cephalonia, Greece, Earthquakes

Georgios Zalachoris, Ph.D.[1]; Dimitrios Zekkos, Ph.D., P.E., M.ASCE[2]; Adda Athanasopoulos-Zekkos, Ph.D., M.ASCE[3]; and Nikos Gerolymos, Ph.D., M.ASCE[4]

Abstract: Following the Cephalonia, Greece, 2014 earthquake sequence ($M_w = 6.1$ and $M_w = 6.0$), liquefaction of gravelly earthfill materials at the ports of Lixouri and Argostoli resulted in the manifestation of ground cracking and coarse-grained soil ejecta, and the quay walls in these ports exhibited lateral ground displacements ranging from 0.1 to 1.5 m. To evaluate the seismic performance of the port quay walls, numerical analyses using the finite-difference method were performed, and the results compared with the observed response. Three commonly used constitutive models (PM4Sand, UBCSand, and URS/ROTH) calibrated based on in situ site investigation data were considered in modeling the liquefiable earthfills. The results of the numerical analyses at both ports using the best-estimate parameters indicate that taller walls exhibit smaller lateral ground displacements than shorter walls, something that is in line with field observations. For the shorter walls, liquefaction-induced lateral spreading played an important role in the observed response, whereas for the taller walls, the seismic behavior is dominated predominantly by the dynamic response of the structural system. PM4Sand and UBCSand models seem to yield very similar deformational results, but the URS/ROTH model, which assigns residual shear strength parameters once liquefaction is triggered, resulted in horizontal displacements that are closer to the observations for short-wall geometries but overpredict the response when the effect of liquefaction on the overall displacements is small. Finally, the numerical analyses demonstrate the strong influence of the pulselike characteristics, as well as the polarization of the input motion on the seismic response of the Lixouri quay walls, indicating that forward directivity contributed significantly to the observed quay wall deformations. **DOI: 10.1061/(ASCE)GT.1943-5606.0002662.** © *2021 American Society of Civil Engineers.*

Author keywords: Quay wall; Dynamic response; Liquefaction; Displacements; Finite difference; Constitutive models.

Introduction: Overview of the 2014 Cephalonia Earthquakes

Cephalonia island, located west of mainland Greece in the Ionian Sea, is characterized by a long history of seismic activity. The region is associated with the highest seismic hazard in Europe, with design acceleration values, as defined by the *Greek Seismic Code* (EPPO 2003), of 0.36 g. The island is near the Cephalonia Transformation Fault (CTF), a seismotectonic feature that connects the Hellenic Arc and the Apulian Microplate (Fig. 1). The CTF is linked to some of the largest seismic events in this region. Overall, 18 earthquakes with magnitudes greater than 6.3 have been recorded since the fifteenth century (GEER/EERI/ATC 2014).

On January 26, 2014, and, again a few days later, on February 3, two major earthquakes occurred near the island of Cephalonia. The first event (January 26, 2014) had a magnitude of $M_w = 6.1$, and the second event (February 3, 2014) was characterized by $M_w = 6.0$. The epicenters and the triggering faults for both earthquakes are shown in Fig. 1(b). In general, across the island, the built environment performed well. Structural damage was not prevalent and, as a result, no fatalities were reported. In contrast, extensive ground failures were documented (GEER/EERI/ATC 2014; Nikolaou et al. 2015; Athanasopoulos et al. 2019), including soil liquefaction, at the port towns of Lixouri and Argostoli, as well as landslides and failures of earth-retaining structures, sculptures, cemetery tombstones, and lifeline networks. These observations were predominantly concentrated in the Paliki peninsula of western Cephalonia. Early observations on the ground indicated that the second event (February 3, 2014) was significantly more damaging than the first (January 26, 2014). Evidence of forward rupture directivity during the second event has been documented (Gazetas and Garini 2017; Garini et al. 2017), something that can partially explain the difference in the level of damage caused by the two earthquakes.

In this study, we focus on the soil liquefaction that was observed at the ports of Lixouri and Argostoli as a result of the 2014 earthquake sequence. Liquefaction caused extensive ground cracking and the manifestation of soil ejecta at the ground surface while also contributing to the lateral ground displacements of the port quay walls in Lixouri and Argostoli ranging from a few centimeters to more than a meter. The investigation of the mechanisms behind the quay wall response is the primary interest of the work presented herein.

In the following paragraphs, we first discuss the recorded strong motions and their characteristics. Then, we present a brief overview of the observed performance of the quay walls and indicate the site locations selected for further analysis. Subsequently, the in situ site investigation efforts that have been undertaken are discussed, and the associated material properties are related to the selected sites.

[1]Geotechnical Engineering Consultant, ElxisGroup, Vasilissis Sofias 54, Athens 11528, Greece (corresponding author). ORCID: https://orcid.org/0000-0001-5561-0058. Email: gzalachoris@elxisgroup.com

[2]Associate Professor, Dept. of Civil and Environmental Engineering, Univ. of California, Davis Hall, Berkeley, CA 94720. ORCID: https://orcid.org/0000-0001-9907-3362. Email: zekkos@berkeley.edu

[3]Associate Professor, Dept. of Civil and Environmental Engineering, Univ. of California, Davis Hall, Berkeley, CA 94720. ORCID: https://orcid.org/0000-0002-3785-9009. Email: adda.zekkos@berkeley.edu

[4]Associate Professor, School of Civil Engineering, National Technical Univ. of Athens, 9 Heroon Polytechniou, Athens 15780, Greece. ORCID: https://orcid.org/0000-0002-3399-561X. Email: gerolymo@mail.ntua.gr

Note. This manuscript was submitted on August 18, 2020; approved on July 1, 2021; published online on September 16, 2021. Discussion period open until February 16, 2022; separate discussions must be submitted for individual papers. This paper is part of the ***Journal of Geotechnical and Geoenvironmental Engineering***, © ASCE, ISSN 1090-0241.

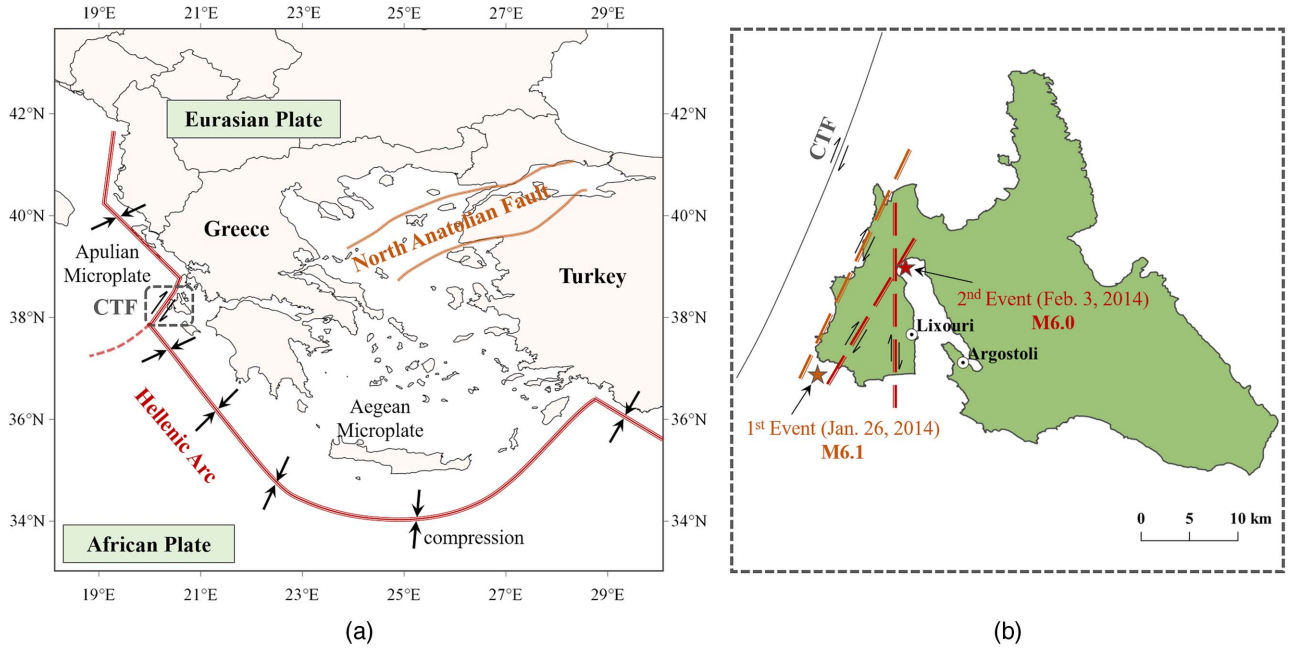

Fig. 1. Maps depicting (a) regional seismotectonic setting; and (b) epicenter locations and associated faults for Cephalonia 2014 earthquake events.

Using these data, numerical models of the quay walls are developed and described in detail. Finally, the results of the numerical analyses are presented and compared with the observed responses, and insights on the physical mechanisms behind the quay wall behavior during the seismic loading are provided.

Strong Ground Motion Recordings in Lixouri and Argostoli

The two Cephalonia 2014 seismic events were recorded by several permanent strong motion stations installed at various locations across Cephalonia island by the Earthquake Planning and Protection Organization - Institute of Engineering Seismology and Earthquake Engineering (EPPO-ITSAK), the National Observatory of Athens - Institute of Geodynamics (NOA-IG), and the University of Patras (UPatras). Of most interest to the present study are the ground motions recorded at the seismic stations located in Lixouri (LXRB) and Argostoli (ARG2). The peak ground accelerations (PGA) observed at these stations for both earthquakes and all three ground motion components [east–west (EW), north–south (NS), and vertical (Z)], are given in Table 1. Additionally, in Fig. 2, the acceleration time histories and the corresponding 5% damped acceleration response spectra for the February 3 record in LXRB and the January 26 record in ARG2 are presented. At both locations, the recording corresponding to the event that yielded the highest PGA values is shown.

As indicated in both Table 1 and Fig. 2, high levels of shaking were recorded during both events. LXRB station recorded larger PGA during the second earthquake (0.67 g), whereas the ARG2 station recorded higher accelerations for the first event (PGA = 0.43 g, for the EW direction), as well as was richer in relatively higher frequencies ($T < 0.3$ s). The ground motion at Lixouri (LXRB) shows a pulselike characteristic in its east–west component (Fig. 2), which translates into significant spectral accelerations (~1.6 g) at long periods ($T \approx 1.3$ s). By comparing the horizontal response spectra of the ARG2 and LXRB records, it can be concluded that the main differences in the spectral shapes are concentrated on the EW components, and not the NS ones. Such observations, when considering the direction of the fault rupture and the proximity of Lixouri to the fault [Fig. 1(b)], are consistent with forward rupture directivity.

Moreover, local soil conditions also contributed to the characteristics of the recorded ground motions in Lixouri (LXRB) and Argostoli (ARG2). Based on in situ V_S measurements presented herein and available in the literature (Karakostas et al. 2014), which will be further discussed in following sections, the inferred average shear-wave velocity at the upper 30 m ($V_{S,30}$) of the soil profile at the recording station locations in Lixouri and Argostoli were estimated to be 256 and 447 m/s, respectively. According to the National Earthquake Hazards Reduction Program (NEHRP) Site Classification system, the Lixouri site consists of stiff soil (Class D), whereas the Argostoli ground motion was recorded on a very dense soil/soft rock site (Class C). Therefore, both recording stations are affected by local soil conditions, i.e., greater amplification of longer spectral periods and deamplification of short spectral periods. Nonetheless, as thoroughly documented by Garini et al. (2017), the recorded EW ground motion in Lixouri (LXRB) shows significant seismological effects of forward rupture directivity, albeit aggravated by soil amplification.

Table 1. Peak ground accelerations for the two events of the Cephalonia 2014 earthquake sequence as recorded at LXRB and ARG2 seismic stations

Recording station	First event (January 26, 2014), M6.1			Second event (February 3, 2014), M6.0		
	EW (g)	NS (g)	Z(g)	EW (g)	NS (g)	Z(g)
LXRB	0.43	0.57	0.57	0.61	0.67	0.53
ARG2	0.43	0.36	0.33	0.24	0.27	0.15

Performance of Quay Walls

As mentioned previously, the 2014 earthquake sequence resulted in significant liquefaction at the ports of Lixouri and Argostoli with manifestation of coarse-grained soil ejecta at several locations near and along the seafronts. The evidence of liquefaction was more pronounced in Lixouri, where the grain size of ejecta had a maximum

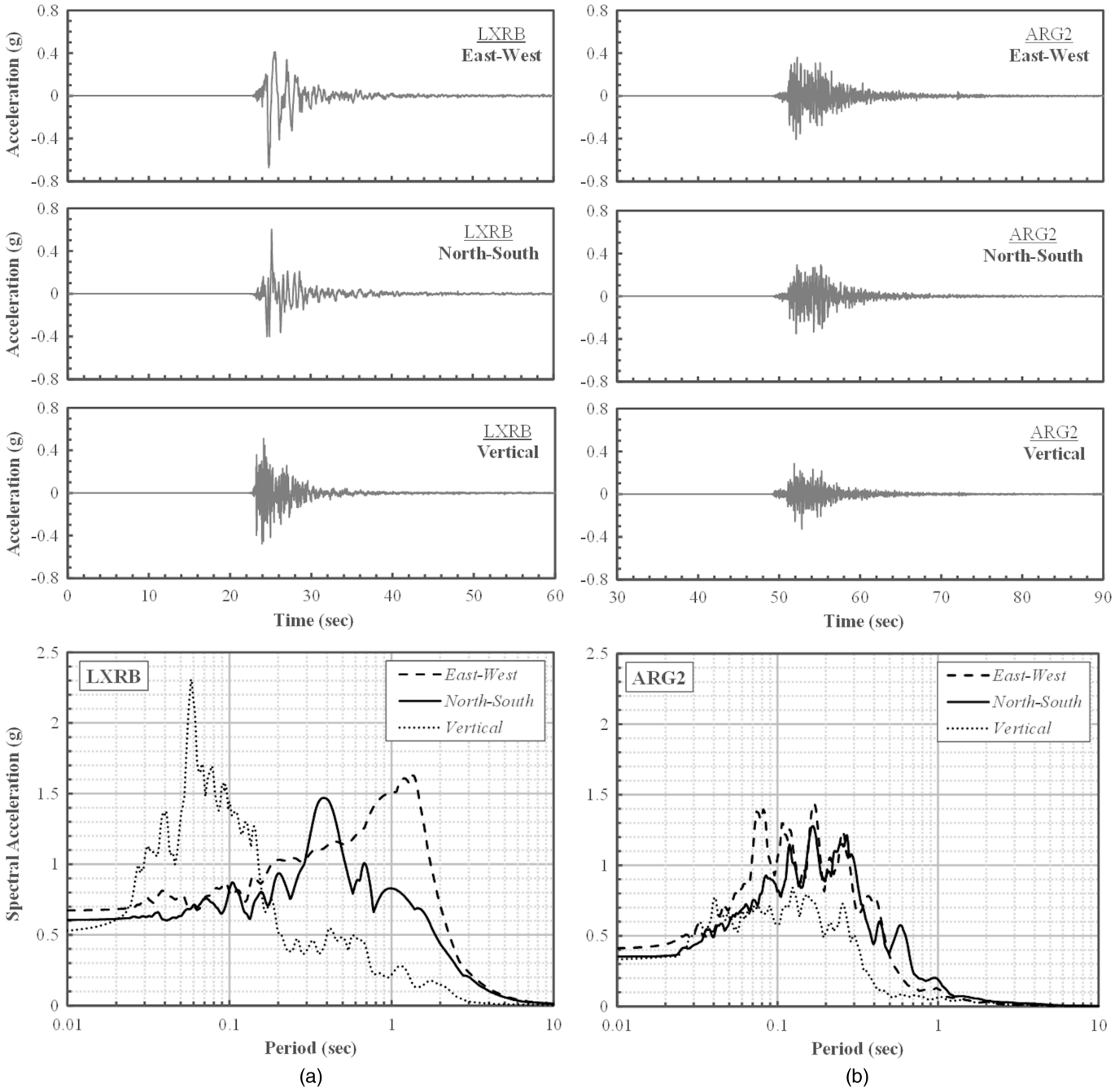

Fig. 2. Three component strong motion recordings and associated 5%-damped acceleration response spectra at seismic stations: (a) Lixouri (LXRB) (February 3 event); and (b) Argostoli (ARG2) (January 26 event).

diameter of 3 cm (Athanasopoulos-Zekkos et al. 2019). The phenomenon has been extensively reported by Geotechnical Extreme Events Reconnaissance/Association/Earthquake Engineering Research Institute/Applied Technology Council (GEER/EERI/ATC 2014) and Athanasopoulos et al. (2019). To evaluate the performance of the quay walls at both ports, Athanasopoulos et al. (2019) measured the lateral ground displacement, as the summation of the observed crack widths, along 24 transects (8 in Lixouri and 16 in Argostoli), with orientation perpendicular to the quay wall fronts, and documented the cumulative horizontal wall displacements. These displacements are a combination of (1) liquefaction-induced lateral spreading, and (2) translational and rotational movement of the quay walls due to the dynamic excitation.

Observations at Lixouri Port

The port of Lixouri (Fig. 3) is characterized by a north–south direction of its main waterfront (main pier). The height of the quay walls is variable (2.6–7.6 m), and the land area behind the walls consists of reclamation fills placed using building debris in the decades following the devastating earthquake of 1953 (Stiros et al. 1994). The distance of the Lixouri port from the causative fault of the February 3 earthquake is approximately 2 km, and LXRB station is located at a distance of ~200 m inland (Fig. 3). Even though manifestation of liquefaction was reported following both earthquakes, most of the lateral movement of the quay walls was a result of the second event.

Fig. 3. Location of strong motion station, selected transects, and site investigation locations at Lixouri port, and observed quay wall damage. (Images by authors.)

Accordingly, Athanasopoulos et al. (2019) reported horizontal displacements at the back face of the walls ranging from 4.3 to 152 cm. The significant variability in the reported values was attributed to the varying height and geometry of the walls, the potential spatial variability of the subsurface conditions, and the physical restraints to translational movement, e.g., the embedment of the wall foundation. Even though lateral ground movement was measured as far back as 90 m behind the quay wall face, most of the displacements occurred within the first 30 m from the waterfront. To further study the physical mechanisms that led to the observed response, this work focuses on three transects documented by Athanasopoulos et al. (2019). Fig. 3 shows the locations of these transects (TS-1, TS-3, and TS-7, hereafter).

The selection was made so that the entire range of wall heights and magnitudes of wall movement was captured. Fig. 3 also depicts the damaged quay walls at the selected locations. The significant spatial variation in the wall displacements is evident; Wall TS-7 experienced very significant damage, whereas Wall TS-3 much smaller indications of lateral spread. Fig. 5 presents the cumulative horizontal displacements along the first 30 m behind the quay wall face at the selected locations.

Observations at Argostoli Port

Similar to Lixouri, the port of Argostoli (Fig. 4) is situated along a subnorth–south orientation. The height of the quay walls at the main pier varies from 4.25 to 8.2 m, and once again, the land behind the seafront consists of material from building debris, reclaimed after the 1953 Cephalonia earthquake. The distance of Argostoli town from the causative fault of the January 26 earthquake was 13 km, and the recording station ARG2 is situated at a distance of ~150 m from the waterfront (Fig. 4).

Athanasopoulos et al. (2019) reported horizontal displacements along four transects within the main pier of the port. The observed movements were ranging from 3.0 to 13.4 cm, values that are significantly smaller than the ones reported in Lixouri. Athanasopoulos et al. (2019) measured lateral movements up to 55 m behind the faces of the quay walls, with most of the lateral spread occurring within the first 30 m (Fig. 5). To evaluate the seismic response of the walls at Argostoli, the present study focuses on the tallest geometry (8.2 m), namely the wall corresponding to Transect 3 (TS-3, hereafter), as documented by Athanasopoulos et al. (2019). Fig. 4 also illustrates the damage caused at the main pier of the Argotoli port by the 2014 earthquake sequence.

Data from Geotechnical and Geophysical Site Investigations

Following the 2014 earthquake sequence, a geotechnical site characterization study was performed at the ports of Lixouri and Argostoli (Geoconsult Ltd. 2016). The goal of the study was the restoration of the quay walls after the significant lateral displacements and rotations they had experienced. This initial site investigation, which took place in March 2014 and April 2016, included 20 boreholes (11 in Lixouri and 9 in Argostoli) and 19 test pits

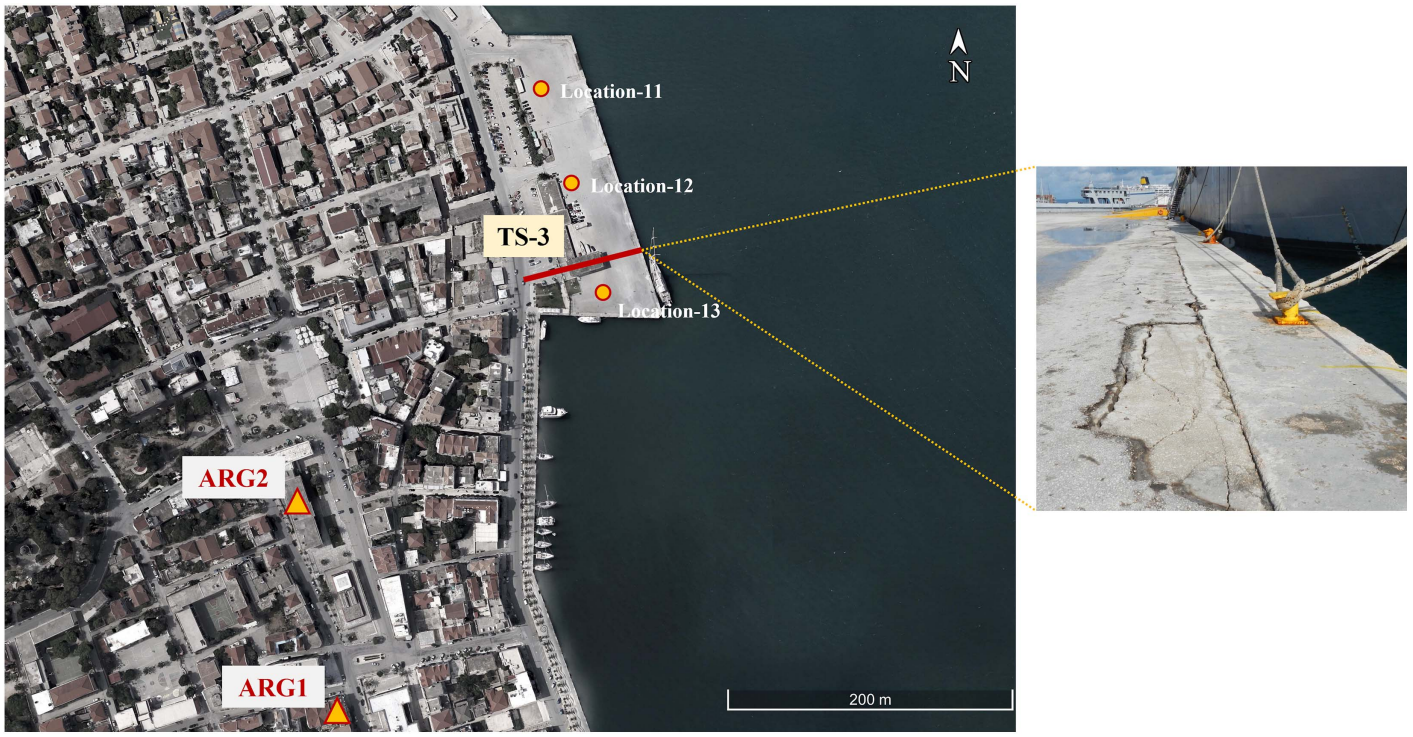

Fig. 4. Location of strong motion stations, selected transect, and site investigation locations at Argostoli port, and observed quay wall damage. (Images by authors.)

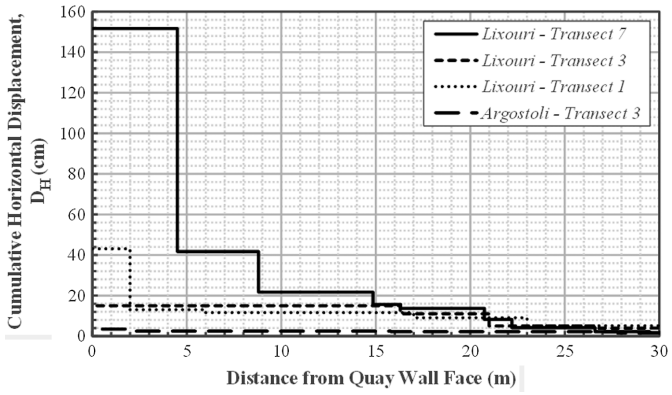

Fig. 5. Distribution of measured cumulative lateral spreading displacements along the selected transects. (Data from Athanasopoulos et al. 2019.)

(13 in Lixouri and 6 in Argostoli). The borings were used to characterize the native soil formations below the quay wall foundations, and the fills behind the quay walls were characterized by the test pits. The sea reclamation fills consist of large stones, with sizes ranging from 10 to 60 cm, in a matrix of finer material of gravels, sands, and low-plasticity silts. In the present study, the data from the initial in situ geotechnical investigation (Geoconsult Ltd. 2016) are primarily used for the development of index properties for the native soil and the reclamation fills. This initial study also provided all the necessary information regarding the quay wall geometries at the selected locations in Lixouri and Argostoli (Figs. 3 and 4).

To better constrain the material behavior and inform subsequent research initiatives, including the present one, in June 2019, Athanasopoulos-Zekkos et al. (2019) further characterized the gravelly reclamation fills at the ports of Lixouri and Argostoli using dynamic penetration testing (DPT), as well as the multichannel analysis of surface waves (MASW) method. Five testing locations were selected in Lixouri, and three DPT and MASW tests were performed in Argostoli (Athanasopoulos-Zekkos et al. 2019). The locations and numbering of these tests are shown in Figs. 3 and 4, respectively. Data from this complementary site investigation effort are used to develop best estimates of the reclamation fill model parameters for the numerical analyses presented herein.

Dynamic cone penetration tests (DPT) were conducted in both Lixouri and Argostoli using the same cone tip described by Cao et al. (2013). DPT was chosen by Athanasopoulos-Zekkos et al. (2019) as an alternative to standard penetration testing (SPT) and cone penetration testing (CPT), which can be unreliable in gravelly deposits. To obtain N'_{120}, the measured DPT blow counts were corrected to account for differences in the rig weight and drop height between the test apparatus used and the one described by Cao et al. (2013). The blow counts were recorded in 10-cm increments as is common with the DPT in China (Cao et al. 2013). Moreover, energy transfer measurements were recorded for each hammer blow for four of the test locations and the energy transfer ratio (ETR) was calculated. Typical ETR values for the DPT drill rig were in the range of 60%–70% with an average value of 65%.

Furthermore, Athanasopoulos-Zekkos et al. (2019) performed MASW tests to develop representative shear-wave velocity (V_S) profiles at selected locations in Lixouri and Argostoli. For the implementation of the method they employed 16 geophones (4.5 Hz), and a 4.5-kg sledgehammer as a source. Data analysis for the MASW measurements consisted of developing dispersion curves from active source signals using the procedure described by Park et al. (1998). The DPT data were used to develop layering for the V_S profiles based on site stratigraphy and were used to constrain the forward modeling analyses and generate more refined estimates of V_S.

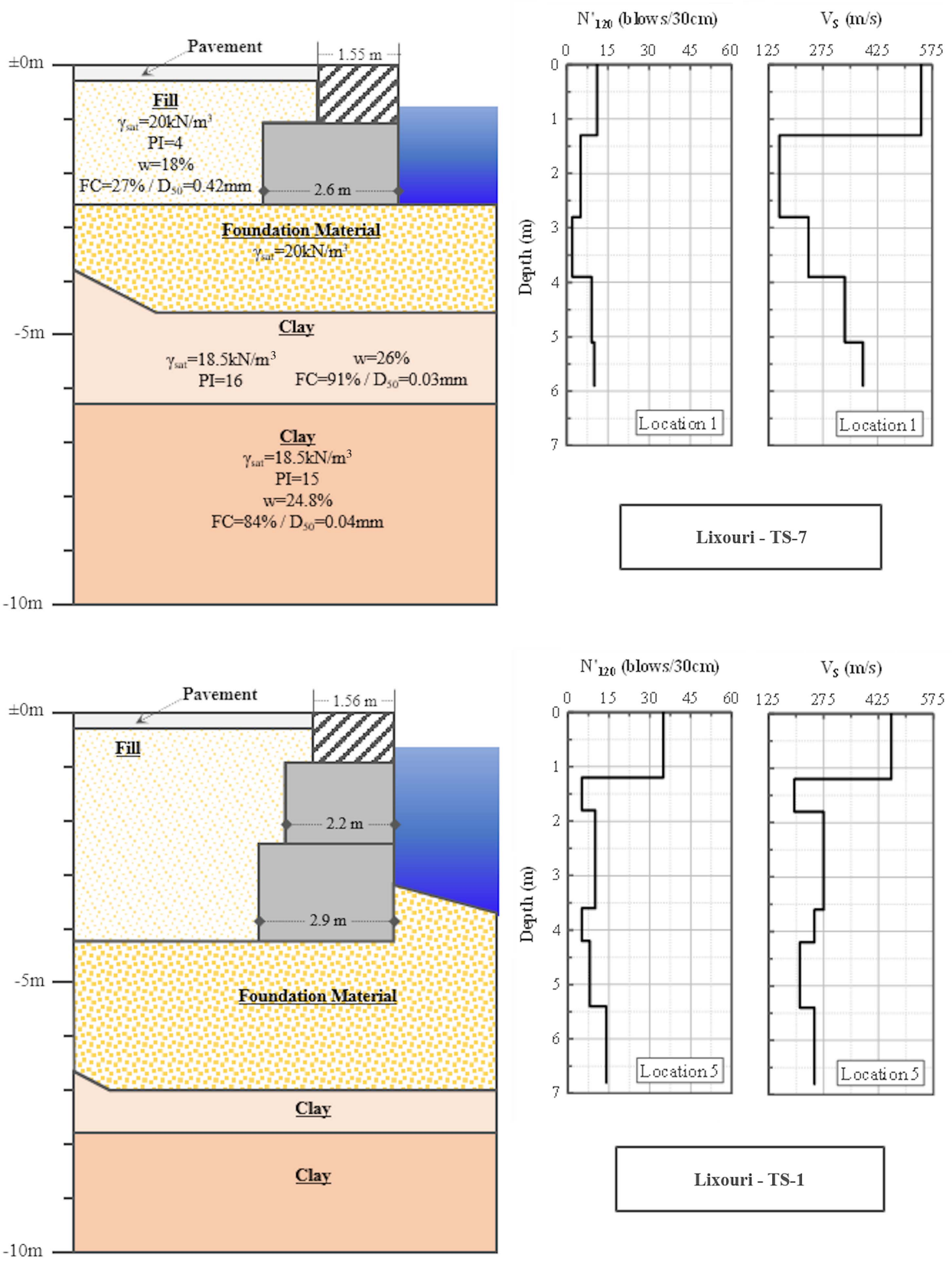

Fig. 6. Wall geometry and data from in situ site investigation at Lixouri TS-7 and TS-1 walls.

Using the information collected by the aforementioned site investigation efforts, representative material properties and wall geometries for all the selected sites in Lixouri and Argostoli were developed. Schematics that depict the soil layering and wall geometries, as well as the corresponding N'_{120} and V_S profiles, at the analyzed quay wall locations are presented in Figs. 6 and 7. The selected wall geometries in Lixouri include a relatively short two-block concrete wall with a height of $H = 2.6$ m (TS-7), an

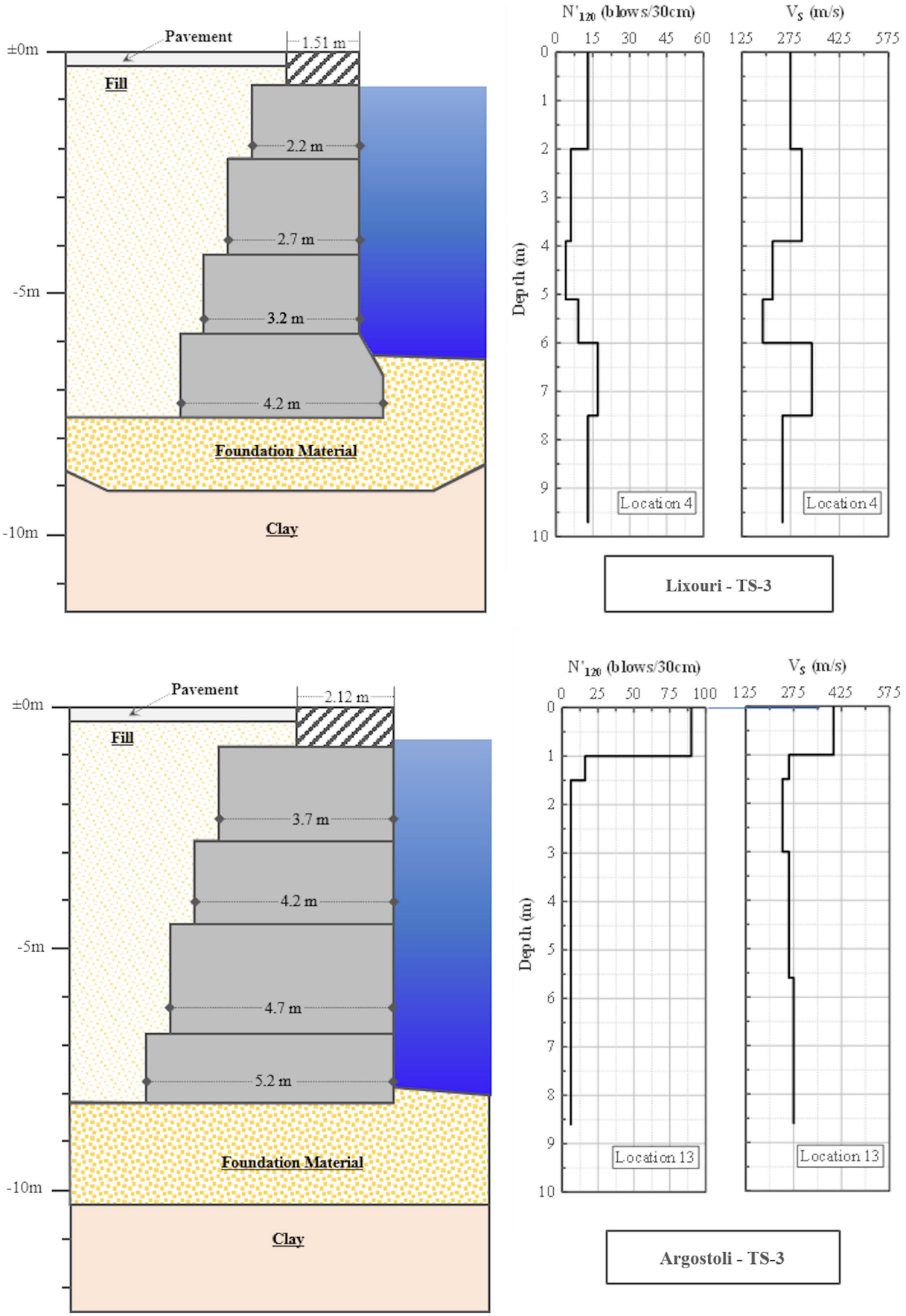

Fig. 7. Wall geometry and data from in situ site investigation at Lixouri TS-3 and Argostoli TS-3 walls.

intermediate sized wall with three concrete blocks and $H = 4.25$ m (TS-1), and a tall wall ($H = 7.6$ m) with five stacks of blocks (TS-3). Similar to the Lixouri TS-3 wall, the selected wall geometry in Argostoli consists of five stacks of concrete blocks with a total height of $H = 8.2$ m (TS-3).

The geologic setting and stratigraphy is similar in both ports. In general, the concrete blocks are founded on medium-dense to dense sand and gravel, with intercalations of cobles of limestone/sandstone origin. The foundation material is underlain by alluvial deposits consisting of low- to medium-plasticity clays (CL) of variable thickness, sandy in places, which are characterized by an ash-green to black-green color (Geoconsult Ltd. 2016). The alluvial deposits, which typically extend inland up to the road that run parallel to the waterfront, are underlain by a stiff cohesive formation extending to the maximum investigated depth.

Numerical Modeling of Quay Walls

The available strong ground motion recordings in the vicinity of the ports, the detailed documentation of the observed response of the port structural systems, as well as the extensive geotechnical and geophysical site investigation data generated, provide a unique opportunity for the assessment of the seismic response of port quay walls. Indeed, the available data consist, holistically, of a well-documented case history that can inform the validation of numerical tools typically employed for computational modeling of physical phenomena in engineering practice.

Herein, we use commonly employed numerical techniques, namely the finite-difference method, to computationally simulate the response of quay walls at the selected locations in Lixouri and Argostoli (Figs. 6 and 7). The following sections present in detail the model geometries, as well as the numerical framework and input motions that provide the basis for the development, calibration, and performance of the computational simulations. The results of these simulations are then discussed and compared with the field observations.

Model Development

For the development of the numerical models, we utilized the two-dimensional, explicit, finite-difference software Fast Lagrangian Analysis of Continua (FLAC) version 8. The materials are represented by rectangular zones, which collectively form a grid that is adjusted to model the wall geometries and stratigraphy at each site (Figs. 6 and 7). The generated model geometries, near the quay walls are illustrated in Fig. 8, and an example of the numerical mesh and the associated idealized stratigraphy, for the Lixouri TS-7 wall is shown in Fig. 9.

The grid consists of zones with an average size of approximately 0.45×0.45 m with a maximum aspect ratio of 2:1. To capture a more detailed distribution of accelerations and stresses at regions of interest, denser zoning was generated behind the quay walls. The maximum frequency considered in the model is $f_{\max} = 50$ Hz, and the average zone height (0.45 m) is smaller than 10% of the wavelength λ associated with the highest frequency component that contains appreciable energy as required for accurate representation of wave transmission through the model (Kuhlemeyer and Lysmer 1973).

The planes on which sliding or separation can occur, namely the horizontal or vertical interfaces between the foundation material or reclamation fill and the concrete blocks, as well as the planes of contact between the stacked wall blocks, are simulated using the interface features available in FLAC. These interfaces are characterized by Coulomb sliding and/or tensile separation and have properties of friction, cohesion, dilation, normal and shear stiffness, and tensile strength. The interfaces that were introduced in the simulations of the present work are annotated in Fig. 8.

We adopted unglued interfaces (no dilation and no tensile strength), with generic values for the normal and shear stiffnesses (10^{10} Pa), and friction angles equal to 30° for the contacts between the concrete blocks, and 0.7 φ (where φ is the effective friction angle of the corresponding soils) for the interfaces between the wall and soil materials (NAVFAC 1986).

Several sensitivity analyses were performed regarding the selected interface stiffness properties, particularly the ones associated with the interface between the concrete blocks. It was found that both the interface friction angle and the values of the interface stiffnesses had a small effect on the computed response, e.g., increasing or decreasing the block-to-block interface friction angle by 10° resulted in less than 10% change in the computed quay wall displacements, on average. The results of these parametric analyses are not included in this study due to space limitations. Accordingly, it was decided that all analyses be performed with the baseline values of interface normal and shear stiffnesses and friction angles listed previously, and the relative differences between the computed responses evaluated on that basis.

Material model properties were selected for each layer based on the data from the site investigation efforts. For the nonliquefiable layers, the input properties consisted of the elastic shear (G), bulk moduli (K), and dry density (ρ_d), and for the materials for which nonlinearities are expected, the effective friction angle (φ) and cohesion (c) were also used. Table 2 summarizes the soil properties attributed to the nonliquefiable soil layers.

Moreover, to account for material degradation and damping during the dynamic excitation, shear modulus reduction and damping curves ($G/G_{\max} - \log\gamma$ and $D - \log\gamma$) were defined for the nonliquefiable materials. Because the response of these materials is found to not be critical for the response of the system, default curves of hysteretic behavior based on the sigmoidal equation with three parameters (sig3), as available in FLAC, were defined. Small-strain damping was also added to the model, i.e., for the liquefiable layers, an additional mass-and-stiffness proportional Rayleigh damping equal to $\xi = 0.5\%$ anchored at $f_{\min} = 1$ Hz was used, whereas for all nonliquefiable zones of the model, a value of $\xi = 1\%$, anchored at $f_{\min} = 1$ Hz, was considered.

To account for the free-field motion that would exist if the models extended infinitely in the horizontal direction, the lateral boundaries are simulated as free-field zones, i.e., the boundaries retain their nonreflecting properties (outward waves are absorbed). Moreover, the lateral boundaries were positioned at a distance from the quay walls such that lateral displacements at the free field remained negligible. All zones below the water table (elevation of -1 m) were considered fully saturated, and the effect of the presence of water at the seaside of the quay walls was modeled via a mechanical hydrostatic pressure applied on the upper-right horizontal and vertical model boundaries. Fluid flow was allowed during the dynamic analyses, whereas hydrodynamic effects due to seawater waves were neglected for simplification purposes.

User-Defined Constitutive Models

The behavior of the liquefiable soil layers that are included in the numerical models, primarily the reclamation fills, is critical to the overall assessment of the seismic response of the quay walls in Lixouri and Argostoli. Thus, the liquefiable fill response is simulated using advanced constitutive models. Three user-defined constitutive models were used within the framework of the present study: (1) PM4Sand version 3.1 (Boulanger and Ziotopoulou 2018),

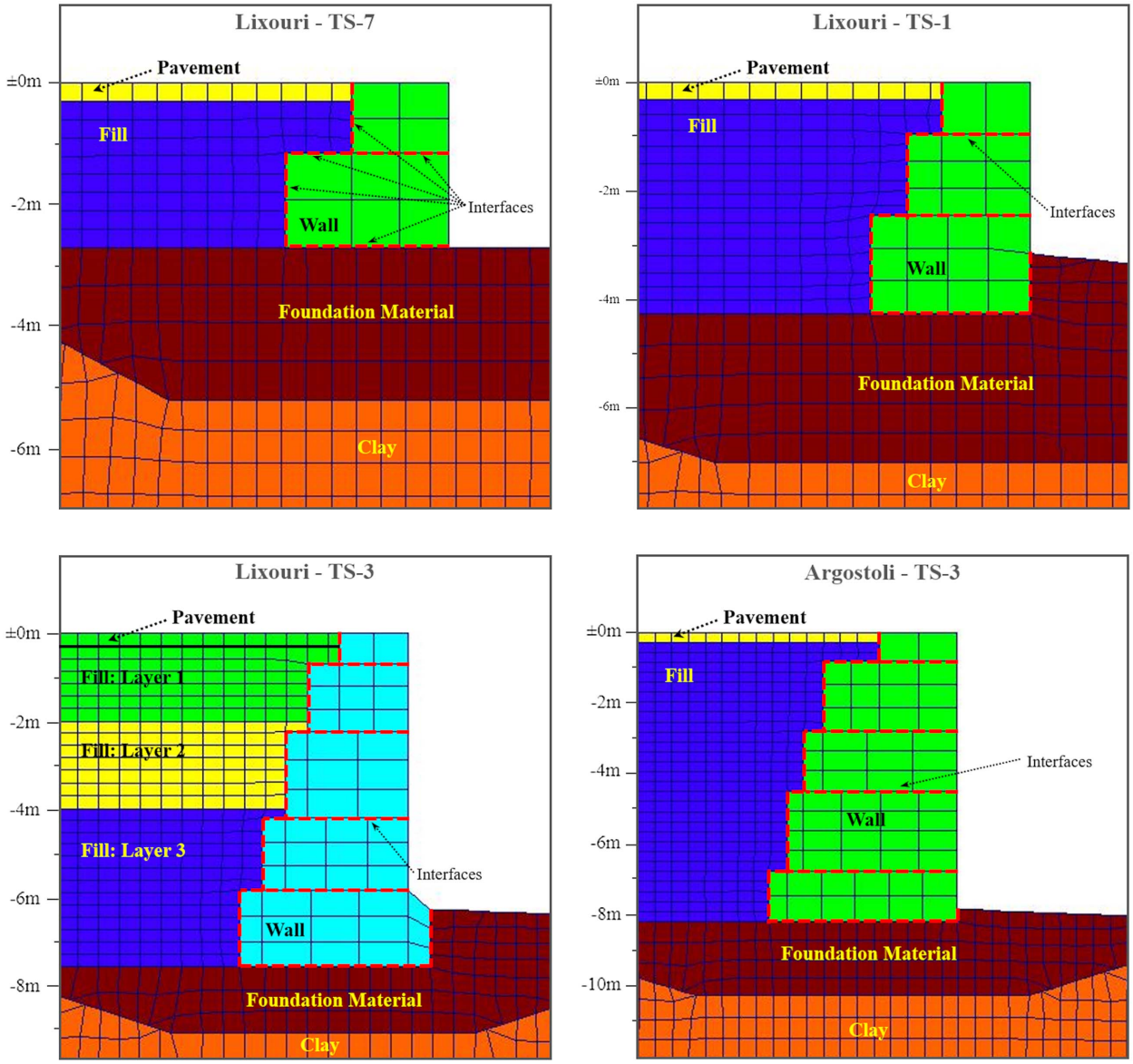

Fig. 8. Numerical model wall geometries for all selected sites.

(2) UBCSand version 904aR (Beaty and Byrne 2011), and (3) URS/ROTH (Dawson et al. 2001; revised 2018). A complete discussion on the characteristics of these models is beyond the scope of this paper, which focuses on the model parameters used and the calibration procedure followed.

The PM4Sand model includes default values for most of its input parameters; only three parameters need to be specified: the relative density D_R, the contraction rate parameter h_{p0}, and the shear modulus coefficient G_0, a parameter related to the small-strain shear modulus ($G_{\max}$). Relative density (D_R) is estimated by correlation to SPT $N_{1,60}$ values [$D_R = \sqrt{N_{1,60}/46}$ (Idriss and Boulanger 2008)]. The coefficient G_0 is obtained by the in situ shear-wave velocity (V_S) measurements because $G_{\max} = \rho \cdot V_S^2$, and h_{p0} is used to modify the soil contractiveness and therefore enable calibration of the models to specific values of cyclic resistance ratio (CRR).

The UBCSand model has 13 input parameters. The elastic shear stiffness (K_G^e) is defined based on in situ shear-wave velocity (V_S) measurements, model calibration to specific values of CRR is performed by varying the bulk stiffness (K_b) parameter, and the remaining parameters are estimated using default calibration correlations with the specified SPT $N_{1,60}$ value.

The URS/ROTH model is a simple formulation built around the Mohr-Coulomb model. It uses a solution procedure to generate pore pressure from shear stress cycles based on the Seed-Idriss cyclic stress approach (Dawson et al. 2001). Once liquefaction is triggered, the material is assigned its residual shear strength, a key model feature that will be discussed further. In this study, when implementing the URS/ROTH model, the residual strength of the liquefied fills is estimated by empirical relationships between the residual shear strength ratio (S_r/σ_v') and the SPT equivalent clean-sand corrected blow count (Boulanger and Idriss 2011).

As discussed previously, Athanasopoulos-Zekkos et al. (2019) performed DPT on the gravelly fill at both Lixouri and Argostoli ports, as an alternative to SPT. The authors also showed that liquefaction-triggering analyses using the DPT data and recommendations by Cao et al. (2013) indicate that liquefaction would be expected at both ports, a finding that corresponds to the field observations. In the present study, the obtained DPT N_{120}'

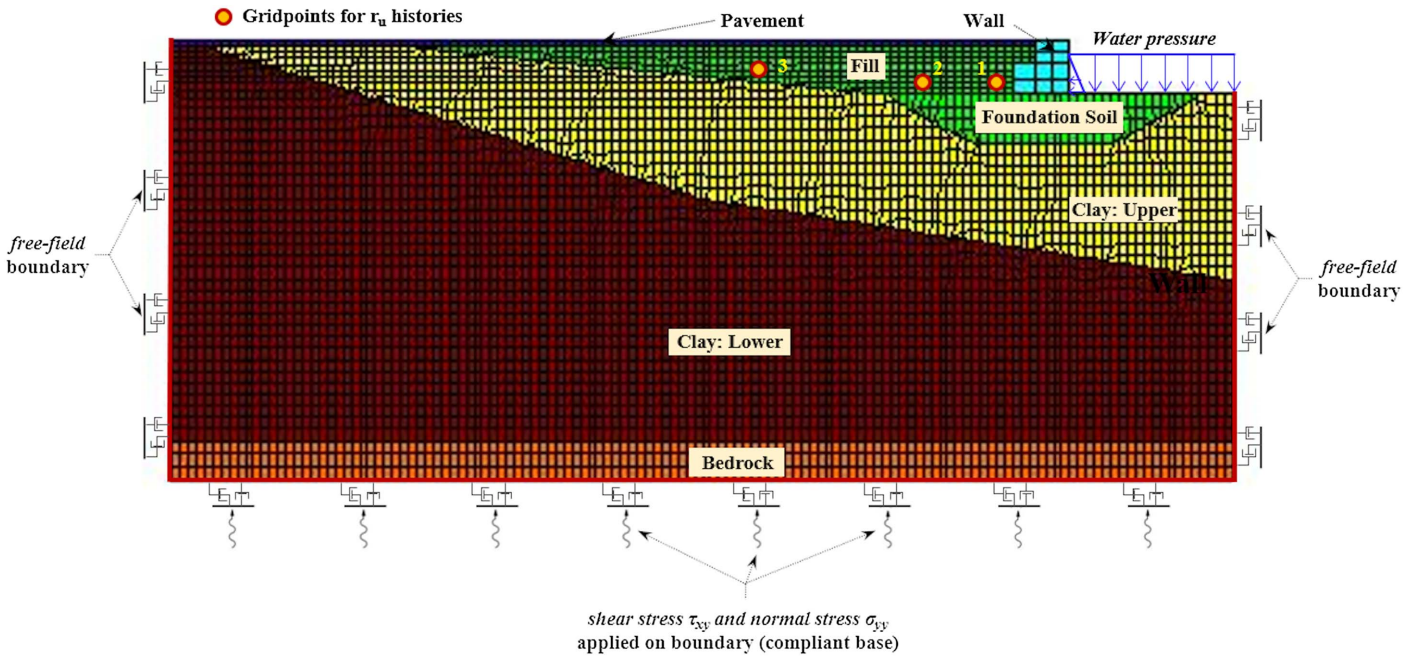

Fig. 9. FLAC mesh, boundary conditions, and application of input motion: example sketch based on Lixouri TS-7 wall.

Table 2. Index properties for all soil layers and model properties attributed to the nonliquefiable soil layers

Material	Model	Dry density, ρ_d (kg/m^3)	Shear modulus, G (Pa)	Bulk modulus, K (Pa)	Friction angle, φ (degrees)	Cohesion, c (Pa)	Porosity, n	Permeability, k (m/s)
Bedrock	Elastic	1,750	4.9×10^8	1.1×10^9	—	—	0.2	1×10^{10}
Quay wall blocks	Elastic	2,300	1.3×10^{10}	1.7×10^{10}	—	—	0.1	1×10^{13}
Pavement	Mohr-Coulomb	2,150	1.3×10^9	1.9×10^9	45	2.0×10^4	0.2	1×10^6
Clay (lower layer)	Mohr-Coulomb	1,482	2.3×10^8	4.9×10^8	30	1.5×10^4	0.35	5×10^{10}
Clay (upper layer)	Mohr-Coulomb	1,468	8.1×10^7	1.8×10^8	35	7.5×10^3	0.4	1×10^{10}
Reclamation fill	User-defined constitutive model	1,695	—	—	33	0	0.3	1×10^4
Foundation soil	User-defined constitutive model	1,600	—	—	32	0	0.4	1×10^6

Note: Permeabilities k were selected based on the model developed by Hazen (1911).

blow counts for the liquefiable layers are converted to equivalent SPT N'_{60} values, and the latter values were adjusted for fines content (Idriss and Boulanger 2008) (Fig. 6) to determine liquefaction triggering. The empirical SPT N'_{60}-DPT N'_{120} correlation proposed by Talbot (2018) was adopted herein. Talbot (2018) used data from four sites in Idaho to develop an overall relationship of $N'_{60} \approx 0.75 \times N'_{120}$. It is worthwhile to mention that the estimated DPT-equivalent N'_{60} values are similar to the V_S-equivalent SPT values computed by utilizing the V_S-N_{SPT} correlation developed based on Greek soil characterization data by Athanasopoulos (1995).

The calibration procedure for PM4Sand and UBCSand involved the variation of model parameters (h_{p0} for PM4Sand and K_b for UBCSand) until the CRR values derived from single element, uniform, cyclic, undrained direct simple shear (DSS) simulations matched the target CRR values for $M_w = 7.5$ and $M_w = 6.0$ (Cephalonia 2014 earthquakes) computed using the SPT-based liquefaction triggering correlation by Idriss and Boulanger (2008). The SPT-based CRR estimates for $M_w = 7.5$ and $M_w = 6.0$ for an effective overburden pressure of 101.3 kPa (1 atm), were assumed to correspond to the simulated CRR for peak shear strain of 3% as well as 15 and 5 equivalent uniform loading cycles (N_{EQ}), respectively. The number of equivalent cycles for $M_w = 6.0$ ($N_{EQ} = 5$) was obtained according to the N_{EQ}-M_w correlation of Seed and Idriss (1982). Examples of single-element DSS responses using the PM4Sand and UBCSand models for the reclamation fill material at the Lixouri TS-7 wall are presented in Fig. 10.

The calibrated PM4Sand and UBCSand model parameters for the associated materials at all wall locations analyzed are tabulated in Tables 3 and 4. Table 4 also includes the URS/ROTH model parameters for the Lixouri TS-7 wall.

Input Ground Motions

The dynamic excitation is applied at the bottom model boundary. In all models, a compliant boundary condition is assumed for the base (i.e., the bedrock is assumed to extend to a significant depth). Accordingly, a quiet (viscous) boundary is assigned along the base of the model in both the x- and y-direction to minimize the effect of reflected waves. The input ground motion is applied as a shear-stress time history, $\tau_{xy}(t)$, along the base (Fig. 9) by converting the Incoming Only part of the bedrock velocity time history, $V(t)$, as follows:

$$\tau_{xy}(t) = -2\rho V_S \cdot V(t) \tag{1}$$

where ρ = dry unit weight of bedrock; and V_S = shear-wave velocity of bedrock.

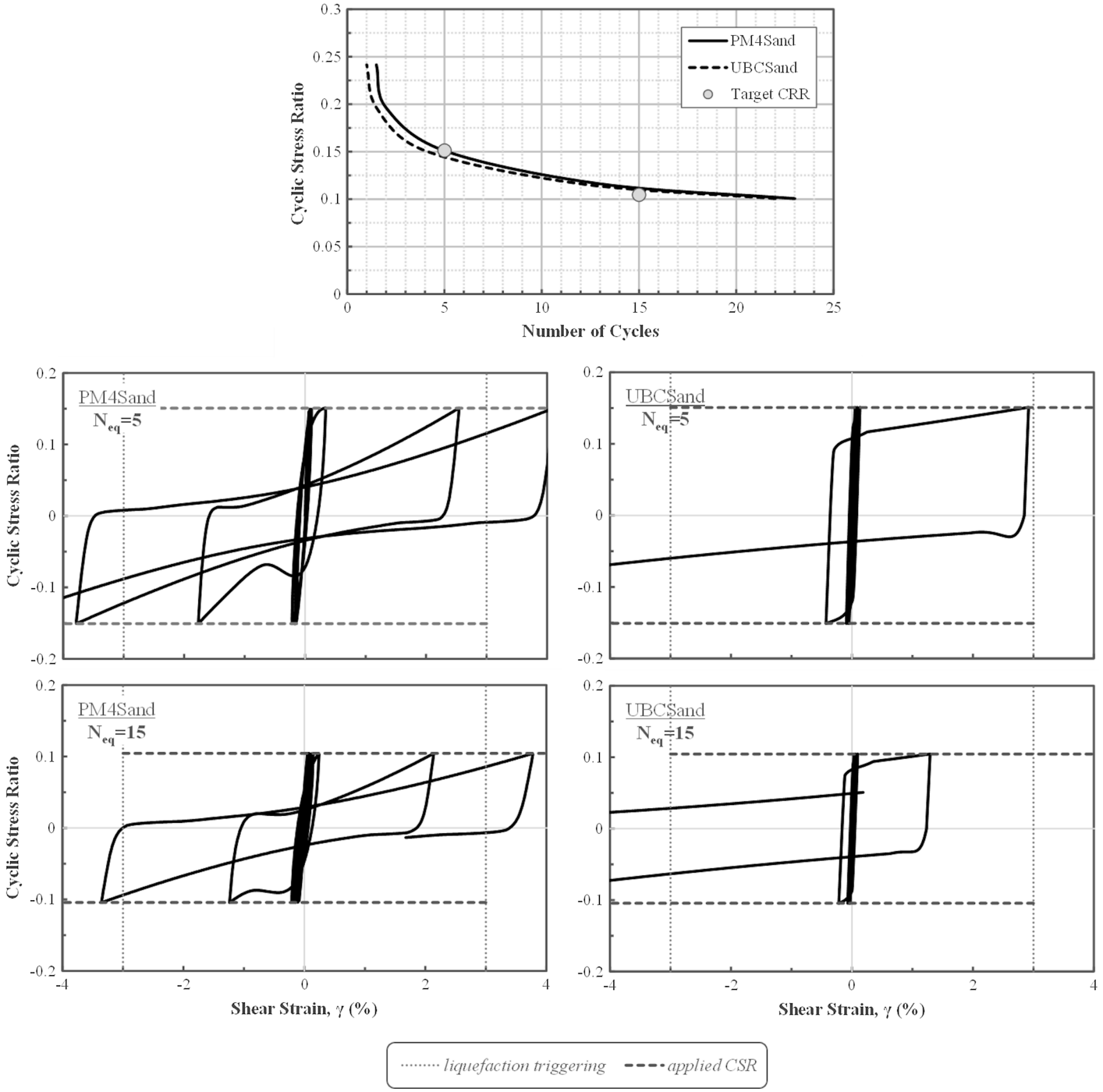

Fig. 10. Response of single soil elements to undrained cyclic simple shear loading: calibration of PM4Sand and UBCSand parameters for the reclamation fill at Lixouri TS-7 wall.

The Incoming Only bedrock velocity time histories in Lixouri and Argostoli are obtained via deconvolution analyses. A shear-wave velocity profile from our team's in situ measurements at the Lixouri Municipality Building and a shear-wave velocity profile reported by Karakostas et al. (2014) for Argostoli, as well as shear modulus reduction (G/G_{max}) and damping (D) curves for plasticity index PI = 30 by Vucetic and Dobry (1991) were considered for the modeling of the alluvial strata in both locations. Reverse one-dimensional (1D) equivalent linear site response analyses were performed using the software STRATA version 0.8.0 (Kottke and Rathje 2008). The recorded EW component of the acceleration records, as previously presented, were input at the surface of the profiles (Fig. 11), and the upward propagating waves at the base were computed.

The resulting Incoming Only bedrock acceleration and velocity time histories are shown in Fig. 12, and the surface and bedrock acceleration response spectra are presented in Fig. 13. To investigate the effect of the intensity of shaking on the response of the quay wall in Argostoli, deconvolution analysis was also performed on the EW acceleration time history recorded at the old ARG1 station (Fig. 4) during the M_S7.0 1983 Cephalonia earthquake (Theodoulidis et al. 2004). The location of ARG1 station is in close proximity (~150 m) to ARG2 (Fig. 4).

Table 3. Calibrated PM4Sand model parameters for the liquefiable layers

Wall	Material	Shear-wave velocity, V_S (m/s)	Corrected blow count, $N'_{60,cs}$ (blows)	Target cyclic resistance ratio ($M_w = 7.5$, $\sigma'_v = 1$ atm), $CRR_{M=7.5}$	Target cyclic resistance ratio ($M_w = 6.0$, $\sigma'_v = 1$ atm), $CRR_{M=6.0}$	Relative density, D_R (%)	Shear modulus coefficient, G_0	Contraction rate parameter, h_{p0}
Lixouri TS-7	Reclamation fill	155	8.0	0.105	0.151	42	403	0.70
	Foundation soil	200	10.1	0.119	0.171	47	592	0.40
Lixouri TS-1	Reclamation fill	195	10.4	0.121	0.175	48	638	0.52
	Foundation soil	250	14.9	0.155	0.224	57	990	0.40
Lixouri TS-3	Reclamation fill (layer 1)	275	18.8	0.192	0.277	64	1,269	0.30
	Reclamation fill (layer 2)	310	24.1	0.271	0.391	72	1,613	0.32
	Reclamation fill (layer 3)	195	10.4	0.121	0.175	48	638	0.52
	Foundation soil	340	28.9	0.424	0.613	80	1,941	0.40
Argostoli TS-3	Reclamation fill	240	14.5	0.152	0.219	56	967	0.34
	Foundation soil	280	18.8	0.191	0.276	65	1,316	0.30

Table 4. Calibrated UBCSand and URS/ROTH model parameters for the reclamation fill, for Lixouri TS-7 wall

Parameter	Symbol	Value
UBCSand		
Shear-wave velocity (m/s)	V_S	155
Constant volume friction angle (degrees)	φ_{cv}	33
Peak friction angle (degrees)	φ_p	33.8
Shear modulus number	k^e_G	403
Bulk modulus	k_b	282
Plastic shear modulus	k^p_G	177
Failure ratio	R_f	0.806
URS/ROTH		
Shear-wave velocity (m/s)	V_S	155
Cyclic resistance ratio ($M_w = 7.5$, $\sigma'_v = 1$ atm)	$CRR_{M=7.5}$	0.105
b-parameter (cyclic strength curve)	b	0.34
Residual shear strength ratio	S_r/σ'_v	0.095

Note: 1 atm = 101.3 kPa.

Based on Figs. 12 and 13, it can be concluded that, similarly to the surface record [Fig. 2(a)], the EW bedrock motion in Lixouri also presents characteristics consistent with forward rupture directivity. A large velocity pulse (Fig. 12) as well as acceleration response spectral values of up to 1.0 g at long periods ($T \approx 1.3$ s) (Fig. 13) are observed. Moreover, the bedrock outcrop motion in Lixouri is much richer in high frequency energy ($T < 0.1$ s) than the surface record, and soil amplification results in larger surface spectral accelerations at $T > 0.1$ s. In contrast, both deconvoluted EW bedrock outcrop motions in Argostoli produce spectral accelerations that are lower than their surface counterpart (Fig. 13). Finally, both records lack the long-period energy of the Lixouri EW motion.

In all analyses, the vertical component of the ground motion was also used as input. Similarly to the horizontal component, the vertical component of input motion is applied as a normal-stress time history, $\sigma_{yy}(t)$, along the base (Fig. 9), by converting the Incoming Only part of the vertical velocity time history, $V_V(t)$, as follows:

$$\sigma_{yy}(t) = -2\rho V_P \cdot V_V(t) \tag{2}$$

where V_P = compression-wave velocity of bedrock.

Results of Numerical Analyses

Computed Response for Best-Estimate Parameters

Using the model geometries, input ground motions, and best-estimate material properties and calibrated constitutive model parameters presented previously, a series of numerical analyses were performed for the selected quay wall locations, namely Walls TS-7, TS-1, and TS-3 in Lixouri, and TS-3 in Argostoli. At first, the collective results, in terms of contours of the excess pore pressure ratio (r_u) at the end of shaking are presented in Fig. 14. The r_u contours overlay the deformed shape of the modeled grid; the relative displacements of the systems can be readily observed. The results are shown only for the PM4Sand model used as the baseline case in this study.

As seen in Fig. 14, zones of excess pore pressure buildup ($r_u > 0.7$) are evident. For the walls in Lixouri, the liquefied reclamation fill zones correspond to the layers with $V_S \leq 200$ m/s (Figs. 6 and 7). In Argostoli, where the reclamation fills are characterized by an almost uniform value of $V_S \sim 240$ m/s, zones with $r_u > 0.7$ are much less pronounced, and even more so for the weaker 1983 motion. This observation is consistent with the post-event reconnaissance that indicated more significant evidence of liquefaction in Lixouri compared with Argostoli during the 2014 Cephalonia earthquake sequence. Correspondingly, Fig. 15 depicts the computed r_u time histories at three selected zones behind the quay walls: one right next to the retaining system (Point 1), one at a free-field zone, at a distance greater than 20 m from the face of the walls (Point 3), and one in a zone in between (Point 2).

The largest values of excess pore pressure ratios are observed in the free field (Point 3), where, for all locations in Lixouri, r_u approaches unity within 2–3 s after the initiation of shaking. For the Argostoli TS-3 wall, the excess pore pressure ratio at the free field only barely becomes larger than 0.7 for the 2014 Cephalonia earthquake, whereas it remains consistently lower than 0.5 for the 1983 seismic excitation, when no liquefaction damage was observed. However, behind the wall (Point 1), much lower r_u values are generated. In fact, for the Lixouri TS-7 location, significant negative excess pore pressure ratios are observed between $t = 5$ and $t = 10$ s of the dynamic input, whereas for both Argostoli analyses, the r_u values recorded at Point 1 take, almost exclusively, negative values. This may seem counterintuitive at first but can be explained

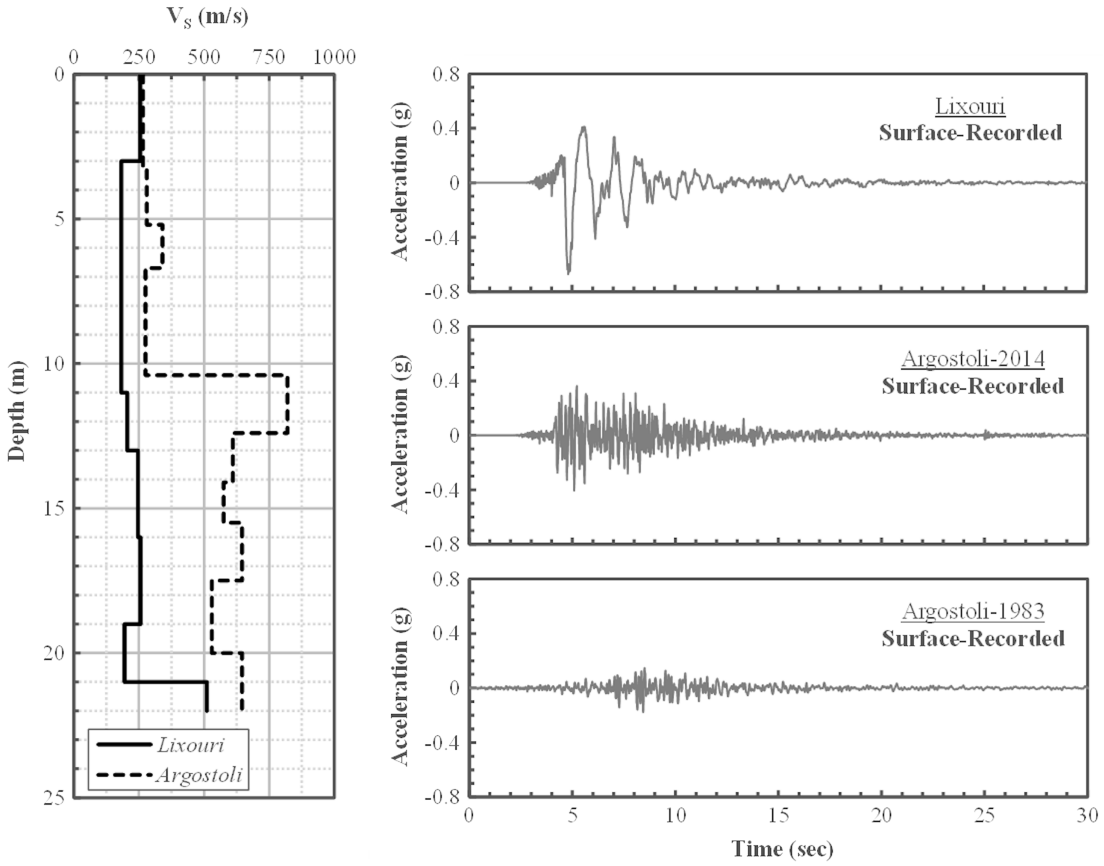

Fig. 11. Shear-wave velocity profiles, and recorded at the ground surface acceleration time histories used for deconvolution analyses at Lixouri and Argostoli ports.

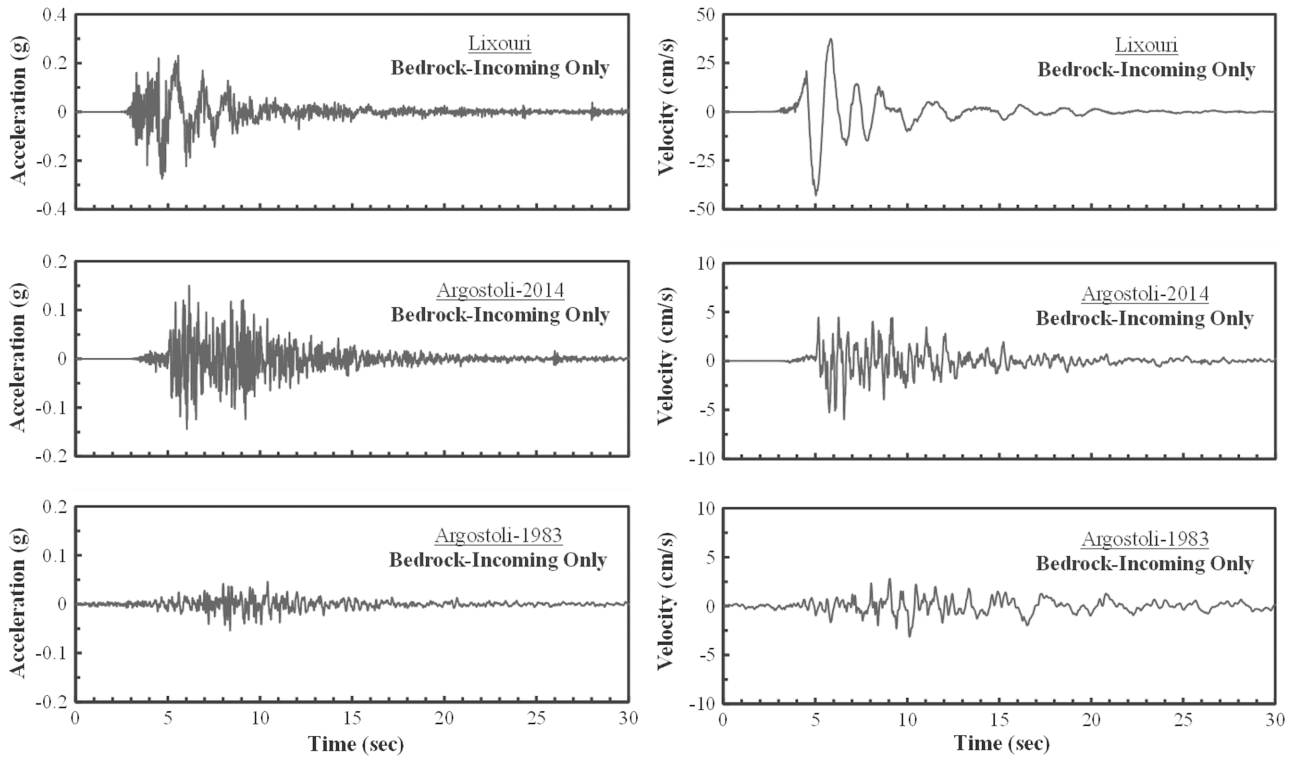

Fig. 12. Deconvolution results: incoming-only bedrock acceleration and velocity time histories at Lixouri and Argostoli ports.

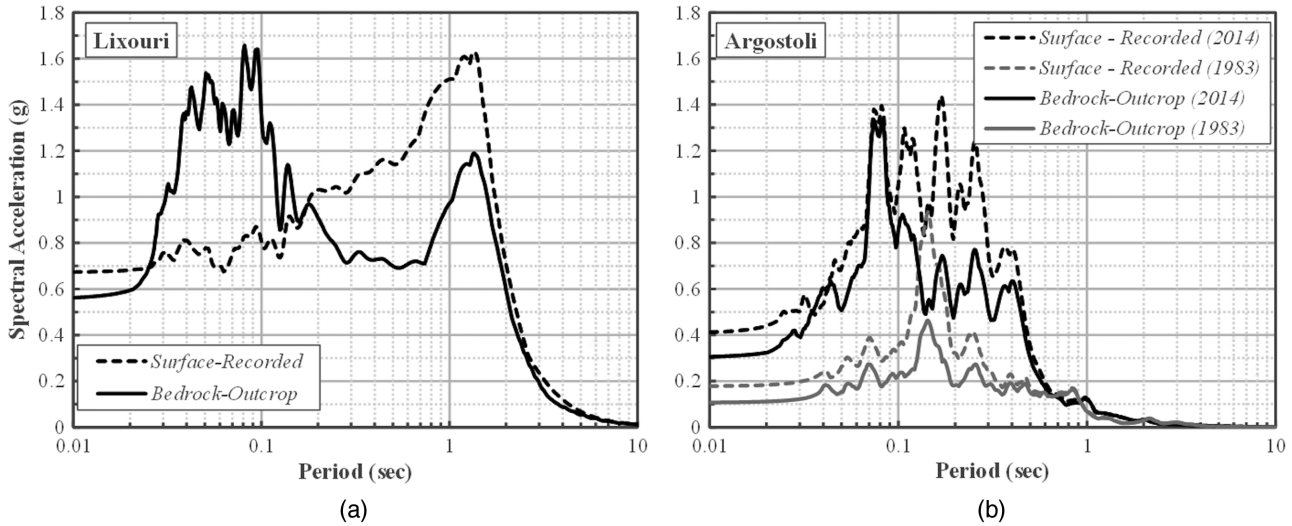

Fig. 13. Deconvolution results: bedrock outcrop and surface acceleration response spectra at (a) Lixouri; and (b) Argostoli ports.

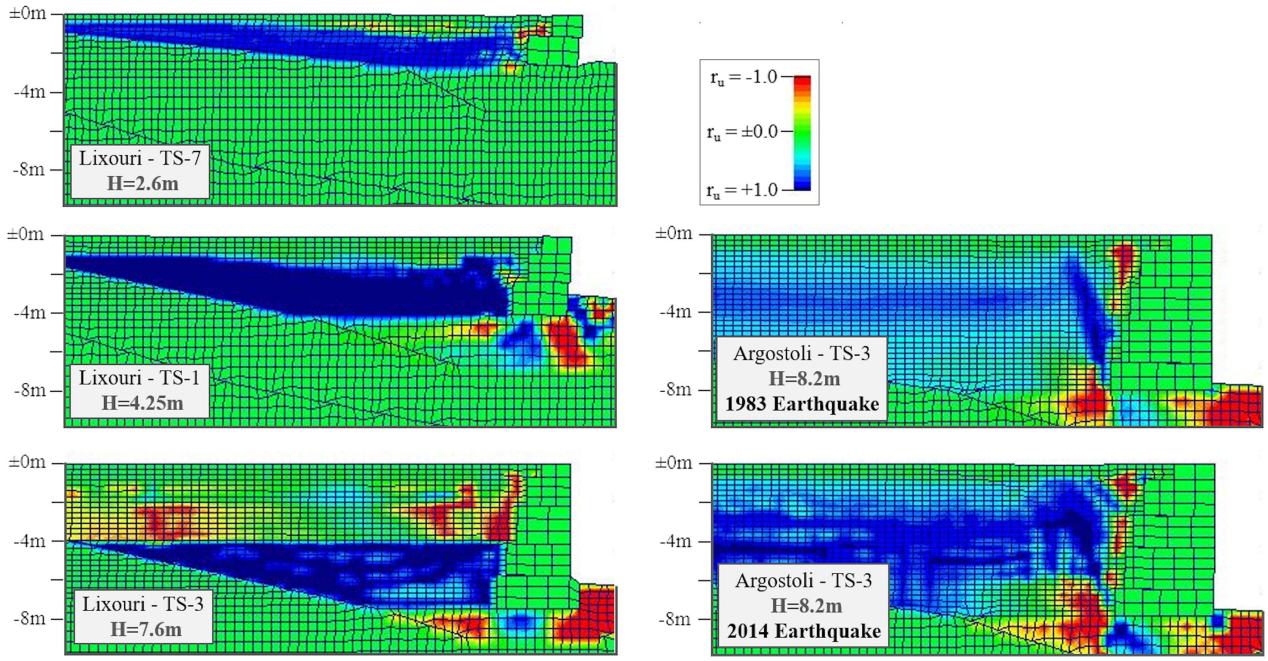

Fig. 14. Computed r_u values behind the quay walls at the end of earthquake shaking at Lixouri and Argostoli ports: PM4Sand and best-estimate parameters.

by the effect of the wall movement on the behavior of the soil mass situated next to it.

Specifically, as the wall undergoes translational and/or rotational movements due to the earthquake shaking, the soil behind it tends to develop negative excess pore pressures and a dilative behavior is triggered. At cases where the contractive behavior is never fully developed (e.g., Argostoli TS-3) due to weaker dynamic excitation, this mechanism prevails, leading to consistently negative r_u values in the vicinity of the base of the structural element. In Lixouri, where the ground motion is strong, negative excess pore pressures are developed at Point 1 simultaneously with the occurrence of excessive wall movements. Once the rate of the displacements of the concrete blocks is reduced (i.e., at $t > 10$ s), r_u becomes again highly positive. Finally, as in Fig. 14, it is observed that the Argostoli TS-3 wall exhibits significantly smaller excess pore pressures under the 1983 earthquake scenario, something that is consistent with the postevent observations, which did not indicate any evidence of liquefaction at the Argostoli port area during the 1983 earthquake (Scordilis et al. 1985).

To compare the seismic responses of the different wall geometries analyzed, Fig. 16 illustrates the displacement time histories as recorded at the crest of the concrete quay walls. The results of the numerical analyses at both ports for the baseline case of PM4Sand and best-estimate parameters indicate that the height of the quay walls plays a significant role in the overall response, i.e., taller walls exhibit smaller lateral displacements. This remark, which is in line with the field observations, can be attributed to two mechanisms: (1) a lateral physical constraint such as the embedment of the wall

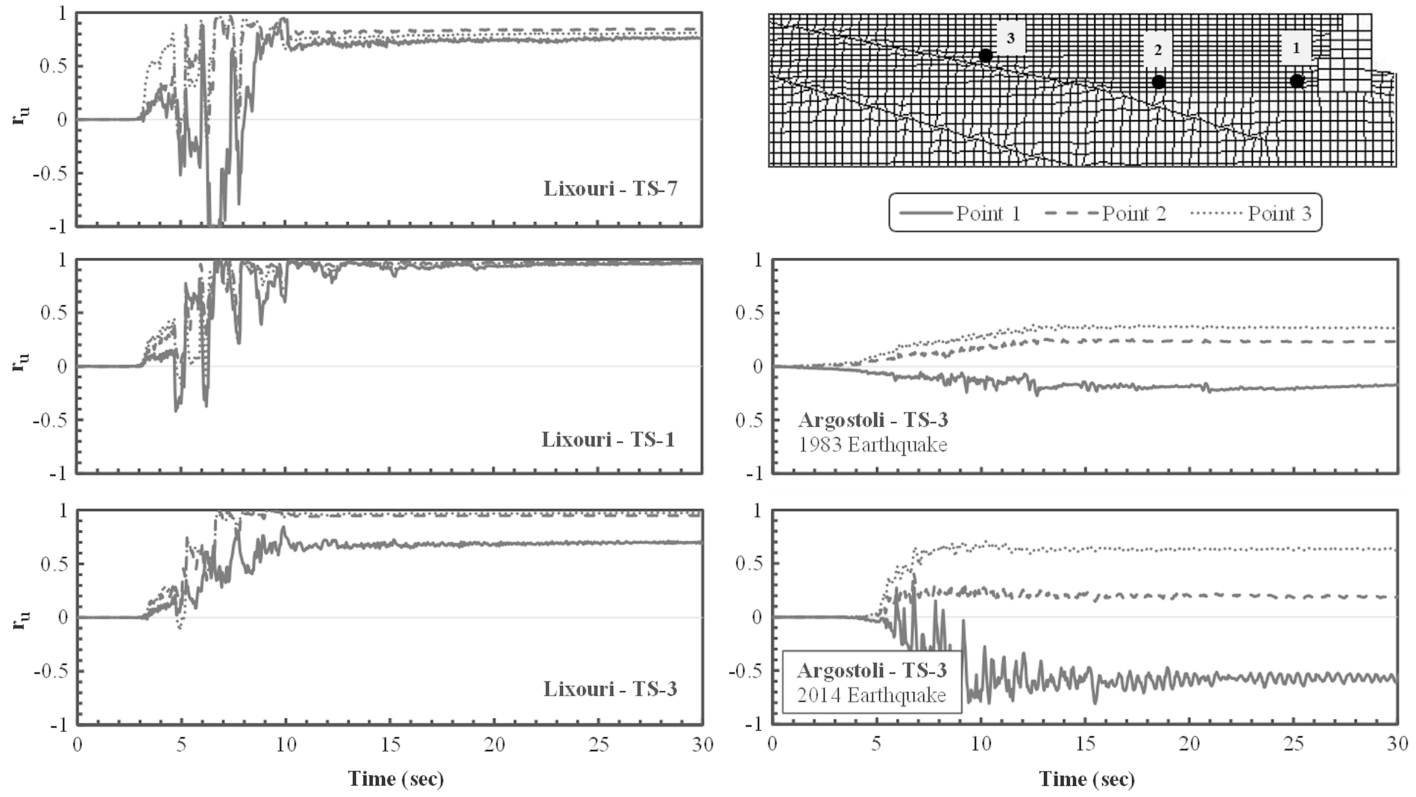

Fig. 15. Computed r_u time histories at three zones behind the quay walls at Lixouri and Argostoli ports: PM4Sand and best-estimate parameters.

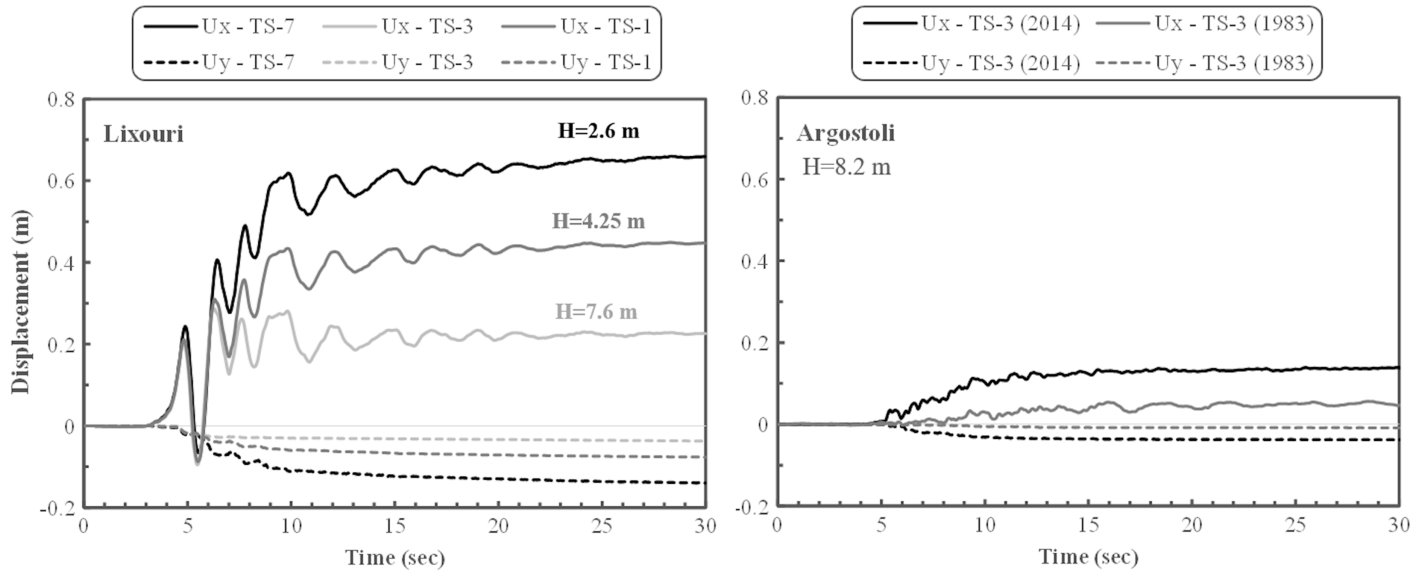

Fig. 16. Computed time histories of horizontal and vertical displacements at the crest of the quay walls at Lixouri and Argostoli ports: PM4Sand and best-estimate parameters.

foundation, and (2) the inertial forces of the port structures. Both factors are exacerbated as the height of the wall increases; typically, foundation embedment is associated with taller walls, which are also characterized by greater inertial forces.

Accordingly, the computed ultimate, maximum displacements for the Lixouri short TS-7 wall ($H = 2.6$ m) are approximately $U_x = 67$ cm, in the seaward horizontal direction and $U_y = 14$ cm in the downward vertical direction (Fig. 16). For the Lixouri tall TS-3 ($H = 7.6$ m) and intermediate TS-1 ($H = 4.25$ m) walls, the corresponding displacement values are approximately: $U_x = 28$ cm and $U_y = 4$ cm, and $U_x = 45$ cm and $U_y = 8$ cm, respectively. In Argostoli, the numerical analyses for the TS-3 wall ($H = 8.2$ m) yield smaller wall crest displacements; the maximum values using the 2014 input motion are $U_x = 14$ cm, $U_y = 4$ cm, $U_x = 6$ cm, and $U_y = 1$ cm when the weaker 1983 record is used. Given that (1) the Argostoli TS-3 wall is slightly taller than the

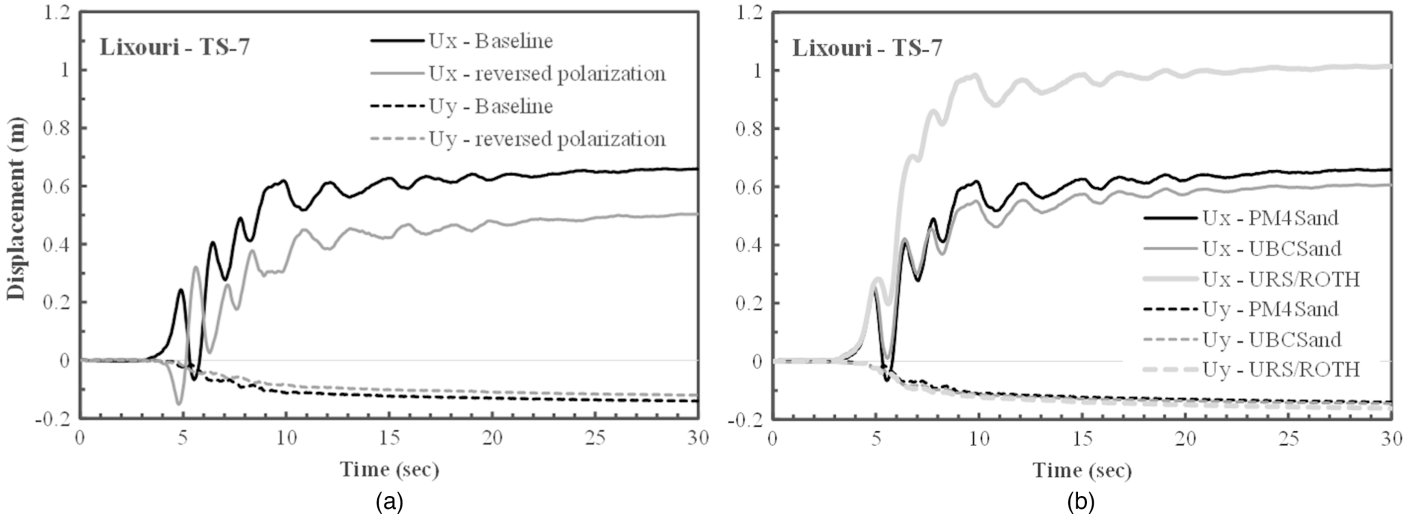

Fig. 17. Computed horizontal and vertical displacement time histories at the crest of the Lixouri TS-7 quay wall: (a) effect of input motion polarization; and (b) comparison between PM4Sand and UBCSand models.

Lixouri TS-3 wall, (2) the ARG2 2014 record is characterized by lower spectral accelerations than the LXRB motion (Fig. 13), and (3) the V_S values of the reclamation fills in Argostoli are larger than in Lixouri (Fig. 7), it can be concluded that the numerical analyses in both ports produce consistent results.

Finally, Fig. 16 also illustrates the effect of the input motion characteristics on the system responses. More specifically, the displacement time histories for the Lixouri quay wall locations show a pronounced steplike form, particularly at $t = 5$–8 s, which understandably coincides with the pulselike characteristic of the input velocity time series (Fig. 12). This steplike form is not present in the deformation responses of the Argostoli TS-3 wall (Fig. 16), highlighting the pronounced effect of forward rupture directivity on the observed response in Lixouri port. The influence of forward rupture directivity on the specific seismic response of the TS-7 wall is also demonstrated by performing the baseline analysis (PM4Sand) using a reversed polarization of the input motion (Fig. 17). In that case, the ultimate maximum displacements of the system are reduced by about 25%, again, proving that the direction and mechanism of the fault rupture (Fig. 1) of the February 3, 2014, event played a significant role in the observed damages at the port of Lixouri.

Finally, Fig. 17(b) illustrates a comparison of the numerical results among PM4Sand, UBCSand, and URS/ROTH models using the best-estimate parameters for the Lixouri TS-7 location (Table 4). The computed wall crest displacements are similar between the PM4Sand and UBCSand models, with differences on the order of less than 10%, indicating that when calibrated against in situ V_S data (Fig. 10), these models yield similar deformational responses. On the other hand, as it will be also discussed in the next paragraph, URS/ROTH results in substantially greater lateral spread than both PM4Sand and UBCSand models, i.e., URS/ROTH estimates horizontal displacements of the TS-7 wall approximately 1.5 times larger than the corresponding values computed based on PM4Sand and UBCSand.

Effect of Liquefaction and Softening

Based on the findings from the previous analyses, additional simulations were performed to isolate and evaluate the contribution of different mechanisms to the observed response. More specifically, the effect of the liquefaction occurrence and the inclusion of a more pronounced loss in strength on the estimated wall crest movements was investigated. Fig. 18 depicts the displacement time histories at the crest of the three Lixouri quay walls resulting from numerical analyses using (1) the baseline PM4Sand model (using best-estimate parameters in Table 4), (2) the PM4Sand model with no liquefaction triggering [PM4Sand (No Liquefaction) in Fig. 18], (3) the PM4Sand model accounting for additional softening [PM4Sand (Softening) in Fig. 18, used only for the TS-7 wall], and (4) the URS/ROTH model (Table 4).

The PM4Sand case without liquefaction occurrence was simulated assuming a fictitious relative density of $D_R = 80\%$ for the reclamation fill that did not allow for pore pressure generation, and the PM4Sand case accounting for additional softening was analyzed by using a reduced contraction rate parameter, $h_{p0} = 0.1$ (instead of $h_{p0} = 0.7$, as in the baseline case). Using $h_{p0} = 0.1$, the corresponding value of CRR is 0.101 for $N_{EQ} = 5$ equivalent cycles ($M_w = 6.0$) compared with a CRR value of 0.151 for the baseline case, i.e., a reduction of approximately 33%.

Based on the numerical results (Fig. 18), it is shown that the contribution of liquefaction of the earthfill to the total lateral deformation of the quay walls is more pronounced in shorter wall geometries (i.e., TS-7); for shorter walls, when liquefaction is not triggered, the computed horizontal displacements are only 30% of the displacements when liquefaction is triggered. As the height of the retaining system increases, the difference in the simulated response between the liquefiable and nonliquefiable cases is reduced. Indeed, for the TS-3 wall ($H = 7.6$ m), the difference between the baseline PM4Sand model results and their counterpart without liquefaction triggering is minimal. Consequently, it can be stated that for the tall wall in Lixouri (TS-3), the prevalent mechanism behind its seismic response, during the Cephalonia 2014 earthquakes, was the dynamic response of the wall rather than the liquefaction-induced lateral spreading.

Finally, based on Fig. 18, it is observed that when the URS/ROTH model is used, the computed horizontal displacements are 1.5 times greater than the baseline PM4Sand case, as mentioned previously, but also ~10% larger than the PM4Sand model with additional softening. These differences can be partially attributed to the fact that the URS/ROTH model assigns residual shear strength parameters once liquefaction is triggered without being able to reproduce cyclic mobility behavior. Therefore, the reclamation fill material becomes overly soft once liquefaction is triggered, resulting in substantially larger deformations than the ones obtained by the PM4Sand model.

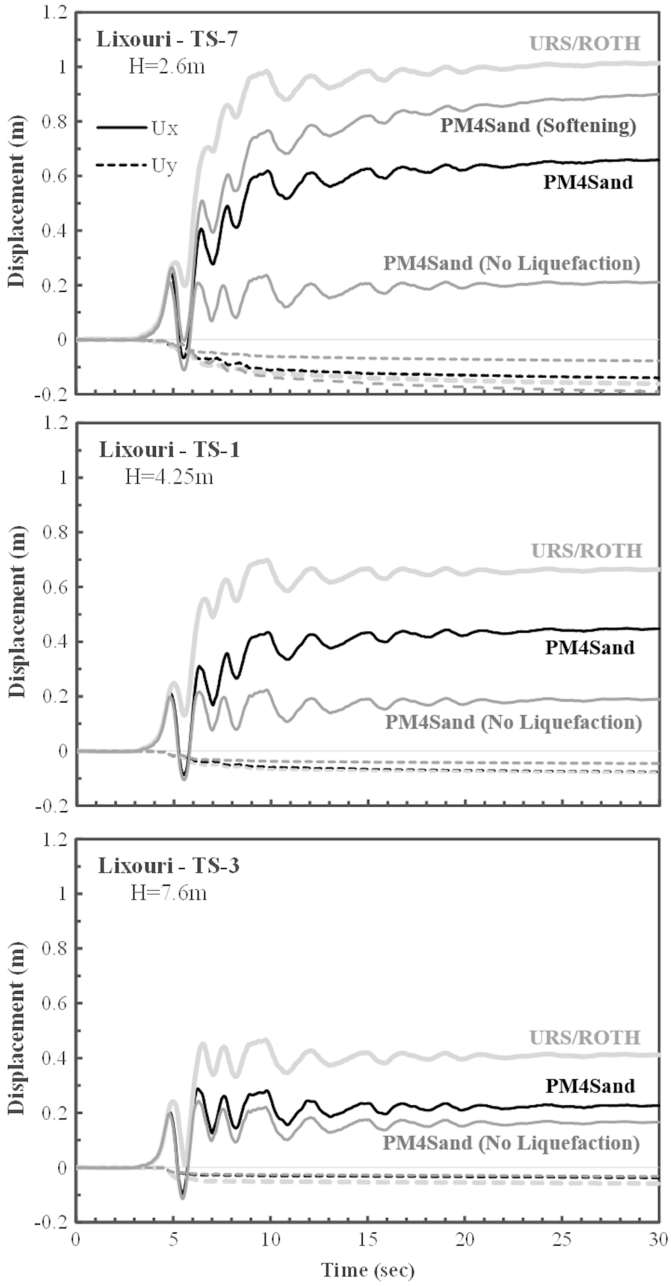

Fig. 18. Computed time histories of horizontal and vertical displacements at the crest of the quay walls at Lixouri: effect of liquefaction and softening.

More specifically, based on single-element, monotonic, undrained DSS simulations for the calibrated baseline case with best-estimate parameters derived from in situ data for the Lixouri TS-7 wall, PM4Sand is producing a shear strength ratio (τ/σ_v') of 0.578 at shear strains of 3%. Similarly, for the PM4Sand case accounting for additional softening mechanisms modeled using a reduced contraction rate parameter, $h_{p0} = 0.1$ (instead of $h_{p0} = 0.7$, as in the baseline case), the developed shear strength ratio (τ/σ_v') at shear strains of 3% is 0.439, which corresponds to a softening of the monotonic undrained stress strain response of 24% relative to the baseline case. Comparatively, for the Lixouri TS-7 wall, the URS/ROTH model was implemented using a residual shear strength ratio (S_r/σ_v') of 0.095 (Table 4), which is assigned once liquefaction is induced, irrespective of the shear strain level.

Comparison of Computed and Observed Responses

The simulation results are compared with the observations documented in the field (Fig. 5). Fig. 19 illustrates the comparison between the observed and the computed wall deformations (D_H), as well as their correlation to the quay wall height (H). The calculated displacements when liquefaction is not triggered and when utilizing the URS/ROTH constitutive framework that introduced residual strength as soon as liquefaction is triggered are also presented. Based on Fig. 19, the effect of the wall height on the seismic response of the quay walls is highlighted. Both the baseline-numerical and the observed responses show that the horizontal displacements become smaller as the wall height increases. Nonetheless, there seems to be no pronounced wall height effect when liquefaction is not triggered; all numerical simulations yield a maximum horizontal displacement of $D_H \sim 20$–30 cm, regardless of the wall height. This value is relatively close to the observed one ($D_H \sim 15$ cm) for the tall wall geometries analyzed (Lixouri and Argostoli TS-3 walls), but substantially underpredicts the observed response for shorter walls ($D_H \sim 43$ cm for TS-1 and $D_H \sim 152$ cm for TS-7). Consequently, it can be concluded that, for the Lixouri TS-7 and TS-1 locations, liquefaction-induced lateral spreading played an important role in the observed response.

Moreover, based on Fig. 19, the baseline PM4Sand model for the shorter TS-7 wall seem to significantly underpredict the field observations in Lixouri (Athanasopoulos et al. 2019). Incorporating residual strength parameters (URS/ROTH) once liquefaction is triggered seems to partially reduce the discrepancy between the observed and baseline-computed response.

Finally, it should be stated that model parameter development, particularly using the SPT N_{60}'-DPT N_{120}' and CRR-$N_{60,cs}'$ correlations—the latter being developed primarily for sands and silty sands—consists of a significant source of modeling uncertainty. To better constrain the computed deformations, Fig. 19 also provides upper/lower bounds of horizontal wall crest displacements estimated by varying up/down the baseline $N_{60,cs}'$ values for the reclamation fill by a factor of 2, which we consider a significant variation, for all Lixouri walls considered, and recalibrating the baseline PM4Sand parameters based on the corresponding target CRR values. Such a large variation (by a factor of 2) of the developed $N_{60,cs}'$ values for the reclamation fill is selected specifically for parametric analyses purposes.

For example, reducing the baseline $N_{60,cs}'$ values for the reclamation fill of the Lixouri TS-7 wall by a factor of 2 results in CRR = 0.109, i.e., a value 28% smaller than the baseline case. Similarly, increasing the baseline $N_{60,cs}'$ values for the reclamation fill of the Lixouri TS-7 wall by a factor of 2 results in CRR = 0.232, i.e., a value 54% larger than the baseline case. As can be seen in Fig. 19, varying the $N_{60,cs}'$ values, and consequently the relative density (D_R), primarily affects the response of the shorter walls (Lixouri TS-7 and TS-1), with the lower bound approaching the No Liquefaction case, whereas the upper bound simulates an even more pronounced softening mechanism. In contrast, for the tall Lixouri TS-3 wall, the variation of the equivalent SPT blow counts did not significantly alter the response, further indicating that for tall-wall geometries, the effect liquefaction-induced lateral spreading is smaller.

Furthermore, given the various uncertainties characterizing the modeling of such complex physical systems as these port structures (i.e., spatial variability of wall and fill characteristics/properties and additional physical constraints or accelerators of wall movement, among others), these analyses should not be seen as a validation or invalidation of any particular numerical model, but rather the

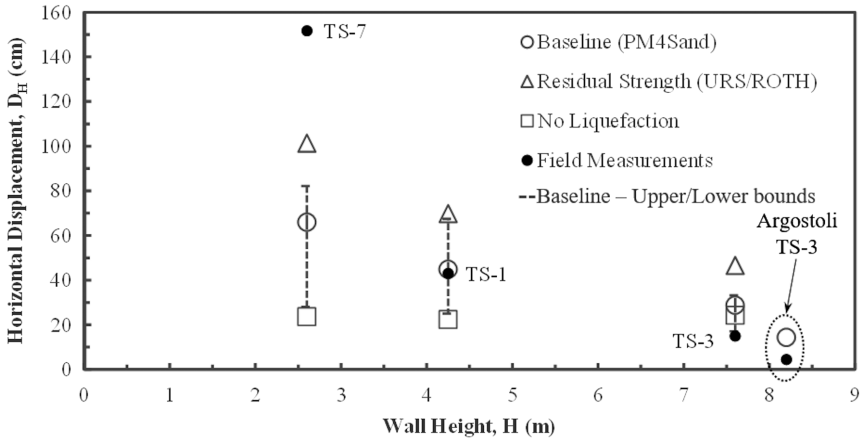

Fig. 19. Comparison between computed and observed lateral wall crest displacements and their correlation to the quay wall height: effect of liquefaction and softening. Upper/lower bounds of the baseline case (PM4Sand) are also depicted.

documentation of several contributing factors to the observed physical response that can guide simulations in geotechnical design practice.

Finally, the contributing factors discussed herein should not be seen, by any means, as the exclusive mechanisms that can possibly explain the observed large quay wall displacements. Other softening mechanisms that cannot be directly captured by the used constitutive models may have contributed, even significantly, to the system response. Such softening mechanisms could be attributed to (1) the multidirectional nature of the actual seismic loading, and (2) the inability of the used constitutive models to adequately simulate the postliquefaction soil behavior. Even though the effects of multidirectional shaking are implicitly incorporated in the case-history SPT-based liquefaction-triggering correlations (Idriss and Boulanger 2008), multidirectional shaking is imposing stress paths that are not reproduced in a single-element test on which the presented calibration procedure is based. Multidirectional shaking has also been consistently shown to decrease the liquefaction resistance of soil (e.g., Pyke et al. 1975; Seed et al. 1975). Moreover, the calibration methodology employed herein relies on soil behavior up to liquefaction triggering and not on the postliquefaction regime, which mostly controls the response at large displacements (Wang et al. 2014; Gerolymos et al. 2019; Tasiopoulou et al. 2020).

Conclusions

The Cephalonia, Greece, 2014 earthquake sequence ($M_w = 6.1$ on January 26 and $M_w = 6.0$ on February 3) (Fig. 1) resulted in extensive damage at the ports of Lixouri and Argostoli. Liquefaction of gravelly reclamation fills resulted in the manifestation of coarse-grained soil ejecta, and the quay walls exhibited lateral ground displacements ranging from 0.1 to 1.5 m (Fig. 5). Informed by strong ground motions recorded at seismic stations at these port towns (Fig. 2), observations from postevent reconnaissance deployments (GEER/EERI/ATC 2014) (Figs. 3 and 4), and data from several site geotechnical and geophysical investigations (Figs. 6 and 7), numerical simulations of the seismic response of several port quay wall systems were performed. Three locations in Lixouri (TS-7, TS-3, and TS-1) and one in Argostoli (TS-3) were modeled (Fig. 8), and three advanced constitutive frameworks were utilized for the simulation of the liquefiable reclamation fills (PM4Sand, UBCSand, and URS/ROTH).

Based on the simulations, it was observed that for the walls in Lixouri, the reclamation fill liquefied at primarily free field zones corresponding to fill layers with V_S less than 240 m/s (Figs. 14 and 15). In Argostoli, where the reclamation fills are characterized by $V_S \sim 240$ m/s, the liquefied zones are less pronounced, an observation that is consistent with the postevent reconnaissance. The results of the numerical analyses at both ports using the best-estimate parameters indicate that the height of the quay walls plays a significant role in the overall response, i.e., taller walls exhibit smaller lateral ground displacements (Fig. 16). This observation is consistent with the field observations and is attributed to two mechanisms: (1) the embedment of the wall foundation at taller wall systems, and (2) the greater inertial forces of taller port structures. PM4Sand and UBCSand models seem to yield very similar deformational results, whereas the effect of forward rupture directivity on the magnitude and characteristics of the seismic response of the Lixouri quay walls was found to be significant (Figs. 16 and 17).

Moreover, it was shown that the contribution of liquefaction to the lateral displacements of the quay walls is more pronounced in shorter wall geometries (Fig. 18). As the height of the retaining system increases, the difference in the simulated response between the liquefiable and non-liquefiable cases is significantly diminished. It was also observed that the URS/ROTH model produces significantly higher horizontal deflections than the PM4Sand and UBCSand models, something that is attributed to the incorporation of residual shear strength parameters once liquefaction is triggered.

Finally, the modeled responses were compared to the observations (Fig. 19). For the shorter walls (TS-7 and TS-1), all numerical models and formulations underpredicted the observed horizontal displacements. Based on the results of the present study, it was concluded that for the Lixouri TS-7 and TS-1 locations ($H = 2.6$ and 4.25 m, respectively), liquefaction-induced lateral spreading played an important role in the observed response, whereas for the Lixouri and Argostoli TS-3 walls ($H = 7.6$ and 8.2 m, respectively), the seismic behavior seems to be dominated predominantly by the dynamic response of the stacked concrete blocks.

Data Availability Statement

Some data used during the study were provided by a third party. Direct requests for these materials may be made to the provider as indicated in the Acknowledgements. Some data that support the findings of this study are available from the corresponding author upon reasonable request.

Acknowledgments

Funding for this study was provided by the National Science Foundation CMMI Grant No. 16632884. Any opinions, findings, and conclusions or recommendations expressed in this material are those of the authors and do not necessarily reflect the views of the National Science Foundation. The authors would like to express their gratitude to Dr. Engineering Seismologist Basil Margaris of the Institute of Engineering Seismology and Earthquake Engineering (ITSAK) for providing the processed ground motions of the Cephalonia 1983 M7.0 earthquake.

References

Athanasopoulos, G. A. 1995. "Empirical correlations vs-NSPT for soils of Greece: A comparative study of reliability." In *Proc., 7th Int. Conf. on Soil Dynamics and Earthquake Engineering*, 19–36. Chania, Crete: Computational Mechanics.

Athanasopoulos, G. A., G. C. Kechagias, D. Zekkos, A. Battilas, X. Karatzia, F. Lyrantzaki, and A. Platis. 2019. "Lateral spreading of ports in the 2014 Cephalonia, Greece, earthquakes." *Soil Dyn. Earthquake Eng.* 128 (Jan): 105874. https://doi.org/10.1016/j.soildyn.2019.105874.

Athanasopoulos-Zekkos, A., D. Zekkos, K. M. Rollins, J. Hubler, J. Higbee, and A. Platis. 2019. "Earthquake performance and characterization of gravel-size earthfills in the ports of Cephalonia, Greece, following the 2014 Earthquakes." In *Proc., 7th Int. Conf. on Earthquake Geotechnical Engineering*. London: CRC Press. https://doi.org/10.1201/9780429031274.

Beaty, M. H., and P. M. Byrne. 2011. "UBCSAND constitutive model version 904aR." Accessed February 4, 2021. https://www.itascacg.com/software/udm-library/ubcsand.

Boulanger, R. W., and I. M. Idriss. 2011. "Cyclic failure and liquefaction: Current issues." In *Proc., 5th Int. Conf. on Earthquake Geotechnical Engineering*. London: International Society of Soil Mechanics and Geotechnical Engineering.

Boulanger, R. W., and K. Ziotopoulou. 2018. *PM4Sand (version 3.1): A sand plasticity model for earthquake engineering applications.* Rep. No. UCD/CGM-17/01. Davis, CA: Center for Geotechnical Modeling, Univ. of California.

Cao, Z., T. L. Youd, and X. Yuan. 2013. "Chinese dynamic penetration test for liquefaction evaluation in gravelly soils." *J. Geotech. Geoenviron. Eng.* 139 (8): 1320–1333. https://doi.org/10.1061/(ASCE)GT.1943-5606.0000857.

Dawson, E. M., W. H. Roth, S. Nesarajah, G. Bureau, and C. A. Davis. 2001. "A practice oriented pore pressure generation model." In *Proc., 2nd FLAC Symp. on Numerical Modeling in Geomechanics*. Rotterdam, Netherlands: A.A. Balkema.

EPPO (Earthquake Planning and Protection Organization). 2003. *EAK: Greek seismic code.* [In Greek.] Athens, Greece: EPPO.

Garini, E., G. Gazetas, and I. Anastasopoulos. 2017. "Evidence of significant forward rupture directivity aggravated by soil response in an Mw6 earthquake and the effects on monuments." *Earthquake Eng. Struct. Dyn.* 46 (13): 2103–2120. https://doi.org/10.1002/eqe.2895.

Gazetas, G., and E. Garini. 2017. "The 2014 Cephalonia twin earthquakes: The seismic failure of memorial columns verify the strong directivity effect." In *Proc., 3rd Int. Conf. on Performance-Based Design in Earthquake Geotechnical Engineering PBDIII*. London: International Society of Soil Mechanics and Geotechnical Engineering.

GEER/EERI/ATC (Geotechnical Extreme Events Reconnaissance Association/Earthquake Engineering Research Institute/Applied Technology Council). 2014. *Earthquake reconnaissance January 26th/ February 2nd 2014 Cephalonia, Greece events*. Cephalonia, Greece: GEER/EERI/ATC.

Geoconsult Ltd. 2016. *Geotechnical report on the assessment of the geotechnical investigation at the port of Argostoli following the Cephalonia earthquakes of January 26 and February 3rd 2014.* [In Greek]. Agia Paraskevi, Greece: Geoconsult Ltd.

Gerolymos, N., M. Anthi, and K. Argyroulis. 2019. "Seismic effective stress analysis of caisson-type quay walls: A comparative study between constitutive models." In *Proc., 7th Int. Conf. on Earthquake Geotechnical Engineering for Protection and Development of Environment and Constructions*, 2608–2615. London: CRC Press. https://doi.org/10.1201/9780429031274.

Hazen, A. 1911. "Discussion: Dams on sand foundations." *Trans. Am. Soc. Civ. Eng.* 73 (11): 199–203.

Idriss, I. M., and R. W. Boulanger. 2008. *Soil liquefaction during earthquakes*. Monograph MNO-12, 261. Oakland, CA: Earthquake Engineering Research Institute.

Karakostas, C., V. Lekidis, K. Makra, B. Margaris, K. Morfidis, C. Papaioannou, M. Rovithis, T. Salonikios, A. Savvaidis, and N. Theodoulidis. 2014. *The earthquake of 26/I/2014 (M6.1) in Cephalonia (Greece): Strong ground motion, soil behavior and response of structures (Preliminary Report)*. Thessaloniki, Greece: Institute of Engineering Seismology and Earthquake Engineering.

Kottke, A., and E. Rathje. 2008. *Technical manual for strata*. Rep. No. 2008/10. Berkeley, CA: Pacific Earthquake Engineering Research (PEER) Center.

Kuhlemeyer, R. L., and J. Lysmer. 1973. "Finite element method accuracy for wave propagation problems." *J. Soil Mech. Found. Div.* 99 (5): 421–427. https://doi.org/10.1061/JSFEAQ.0001885.

NAVFAC (Naval Facilities Engineering Command). 1986. *Foundations and earth structures: Design manual*. Alexandria, VA: NAVFAC.

Nikolaou, S., D. Zekkos, D. Asimaki, and R. Gilsanz. 2015. "Reconnaissance highlights of the 2014 sequence of earthquakes in Cephalonia, Greece." In *Proc., 6th Int. Conf. on Earthquake Geotechnical Engineering*. Christchurch, New Zealand: International Society for Soil Mechanics and Geotechnical Engineering.

Park, C. B., R. D. Miller, and J. Xia. 1998. "Imaging dispersion curves of surface waves on multi-channel record." In *SEG technical program expanded abstracts*, 1377–1380. Tulsa, OK: Society of Exploration Geophysicists.

Pyke, R., B. Seed, and C. Chan. 1975. "Settlement of sand under multidirectional shaking." *J. Geotech. Eng. Div.* 101 (4): 379–398. https://doi.org/10.1061/AJGEB6.0000162.

Scordilis, E. M., G. F. Karakaisis, B. G. Karakostas, D. G. Panagiotopoulos, P. E. Comninakis, and B. C. Papazachos. 1985. "Evidence for transform faulting in the Ionian Sea: The Cephalonia island earthquake sequence of 1983." *Pure Appl. Geophys.* 123: 388–397. https://doi.org/10.1007/BF00880738.

Seed, H. B., and I. M. Idriss. 1982. *Ground motions and soil liquefaction during earthquakes.* Oakland, CA: Earthquake Engineering Research Institute.

Seed H. B., I. M. Idriss, F. Makdisi, and N. Banerjee. 1975. *Representation of irregular stress time histories by equivalent uniform stress series in liquefaction analysis.* Rep. No. EERC 75-2. Berkeley, CA: Earthquake Engineering Research Center, College of Engineering, Univ. of California.

Stiros, S., P. Pirazoli, J. Laborel, and F. Laborel-Deguen. 1994. "The 1953 earthquake in Cephalonia (Western Hellenic Arc): Coastal uplift and halotectonic faulting." *Geophysics* 117 (3): 834–849. https://doi.org/10.1111/j.1365-246X.1994.tb02474.x.

Talbot, M. H. 2018. "Dynamic cone penetration tests for liquefaction evaluation of gravelly soils." Ph.D. dissertation, Dept. of Civil and Environmental Engineering, Brigham Young Univ.

Tasiopoulou, P., K. Ziotopoulou, F. Humire, A. Giannakou, J. Chacko, and T. Travasarou. 2020. "Development and implementation of semiempirical framework for modeling postliquefaction shear deformation accumulation in sands." *J. Geotech. Geoenviron. Eng.* 146 (1): 04019120. https://doi.org/10.1061/(ASCE)GT.1943-5606.0002179.

Theodoulidis, N., I. Kalogeras, C. Papazachos, V. Karastathis, B. Margaris, C. Papaioannou, and A. Skarlatoudis. 2004. "HEAD v1.0: A unified Hellenic accelerogram database." *Seismol. Res. Lett.* 75 (1): 36–45. https://doi.org/10.1785/gssrl.75.1.36.

Vucetic, M., and R. Dobry. 1991. "Effect of soil plasticity on cyclic response." *J. Geotech. Eng.* 117 (1): 89–107. https://doi.org/10.1061/(ASCE)0733-9410(1991)117:1(89).

Wang, R., J.-M. Zhang, and G. Wang. 2014. "A unified plasticity model for large post-liquefaction shear deformation of sand." *Comput. Geotech.* 59 (Jun): 54–66. https://doi.org/10.1016/j.compgeo.2014.02.008.